Received: December 18, 2024. Revised: January 12, 2025.

INASS

International Journal of
Intelligent Engineering & Systems

http://www.inass.org/

Generalized Joint Subcarrier-Time Index Modulation Aided Differential Chaos Shift Keying System

Muntaha Kadhum Musa[1]* **Fadhil S. Hasan[1]**

[1]*Department of Electrical Engineering, Al-Musansiriyah University, Iraq*
*Corresponding author's Email: *muntaha.kadhum@uomustansiriyah.edu.iq*

Abstract: This paper presents a new dual index modulation system termed the Generalized Joint Subcarrier-Time - Index Modulation DCSK (GJSTIM-DCSK) scheme, intended to enhance spectral efficiency and data-transmitted rate of the recent dual index-DCSK modulation schemes. Efficiently employs two transmitter resource entities presented by subcarrier and time slot, facilitating effective transmission at elevated data rates. Moreover, this system consists of 2^q+1 subcarriers; one of them is used to carry a chaos reference signal after repeated M_s times, and the others are divided equally to N_s subcarriers in each group. The k-combinatorial mapping is utilized to choose N_c active subcarriers from N_s according to x_s subcarrier index bits, and select M_c time slot from M_s in each inactive subcarrier according to x_t time slot index bits. Additional to index bits, there are $N_c M_s + (N_S - N_C)(M_S - M_C)$ DCSK modulated bits, first$(N_c M_s)$bits are modulated by c_x chaos reference signal carried by N_c active subcarriers, and also last $(N_S - N_C)(M_S - M_C)$bits are modulated by orthogonal copy of chaos reference generated using Hilbert transform and carried by unselected time slots of inactive subcarriers. Our analysis encompasses the system's transmission bit rate, bandwidth efficiency and complexity, contrasting these functions against to analogous systems. The suggested system improves bandwidth efficiency by approximately 1.33, 1.45 and 5.5 times greater than that of GFTIM-DCSK-II , CTIM-DCSK and GSPIM-DCSK-II, respectively with N_s=16, N_c=1, $M_s = 16$, $M_c = 4$, and G=2. Furthermore, we devise mathematical BER (Bit Error Rate) theory for the GJSTIM-DCSK scheme with the presence of AWGN (Additive White Gaussian Noise) and multipath fading channels with Rayleigh distribution. The simulation findings not only validate the fidelity of the mathematical BER expression but also demonstrate the system's enhanced BER performance compared to analogous systems under comparable environment. For example, with M_s =4 and BER=10^{-3} under both additive noise and Rayleigh channels, the GJSTIM-DCSK system exhibits an estimated 2 dB gain over the GFTIM-DCSK-II, while showing gains of 1 dB and 2.5 dB over the GSPIM-DCSK-II in AWGN and Rayleigh fading channels, respectively.

Keywords: Joint subcarrier-time index modulation, K-combinatorial method, DCSK, High data rate, Multipath rayleigh fading channel.

1. Introduction

When employed as spreading codes, chaotic signals provide numerous advantages over conventional approaches in the context of wideband communication systems; because these signals are nonperiodic, broad-spectrum, uncorrelated, anti-interference, and harder to forecast, restore, .and present greater challenges for characterization than periodic carriers. Additionally, the information that is modulated by chaotic signals is extremely difficult to decipher due to their unique properties [1- 3]. Therefore, chaotic communication is regarded as an advantageous approach to address the diverse obstacles posed by wireless communication, garnering increasing attention [4, 5]. In recent years, an abundance of digital communication methods based on chaos has been introduced. The need to create a synchronized replica of the chaos signal at the receiving station has led to the categorization of these systems into coherent and noncoherent schemes [6].

Differential-chaos-shift-keying (DCSK) in [7] is the most extensively researched noncoherent system,

as it does not require the generation of a synchronous replica of the nonperiodic chaos signal at the demodulator. However, achieving synchronization is particularly challenging in noisy channels due to the "sensitive dependence on initial conditions" inherent in chaotic signals. Also, the DCSK technique possesses the advantage of inherent multipath variety, leading to reliable performance in multipath channels [8]. Several applications have made use of DCSK schemes, including multiple-input multiple-output (MIMO) technologies [9], ultra-wideband in dense-multipath communication [10, 11], network coding technique in communication networks [12], cooperative communication networks [13- 15], power line communications [16, 17], and underwater acoustic communications [18]. These developments have significantly broadened the scope of DCSK applications. In [7], the reference sequences and modulated signal are transmitted in discrete time slots for each bit duration, resulting in a fifty percent decrease in transmission bit rate and bandwidth efficiency in comparison to a coherent chaotic communication schemes, such as CSK [19]. Therefore, numerous noncoherent DCSK systems have been investigated to address the DCSK's constraints. In high-efficiency DCSK (HE-DCSK) [20], the spectral efficiency is doubled through carrying two information bits in a single modulation interval. In order to eliminate the requirement for RF lines delay in DCSK transceivers, [21- 24] proposed systems employ Walsh codes to discriminate between chaotic sequences and modulated information signals. An improved noncoherent scheme (I-DCSK) has been proposed in [25], which increases the transmission bit rate to double and enhances the bandwidth efficiency through using the time reversal operation. The M-ary architecture with DCSK and CS-DCSK schemes is proposed in [26- 29], which employs various novel Techniques to improve system's energy consumption and bit rate.

In [30], a multi-carrier-DCSK (MC-DCSK) modulation is implemented to attain an optimal balance between reliability, low- Energy consumption, and high bit rates by transmitting multiple DCSK bits across the available subcarriers. A method of RM-DCSK (reference-modulated-DCSK) was explored, whereby the chaotic wavelet serves as both a reference and a transmitter of information bits [31]. Moreover, a short-reference-DCSK system (SR-DCSK) was introduced in [32], this approach is used short reference sequences, result in increased transmission bit rate and improved energy efficiency. The Gram-Schmidt- technique is utilized in [33, 34] as a substitute of Walsh code for simultaneous transmission of several bits at the same time interval. To mitigate the noise variation that effects on the received wavelet and improve BER performance, a noise-reduction-DCSK (NR-DCSK) approach is investigated in [35], in which chaotic signal are produced and subsequently replicated P times for every transmitted bit. To further improve the bandwidth and energy efficiency and transmission bit rate of DCSK systems, orthogonal-frequency- division multiplexing (OFDM) is utilized. There are several kinds of hybrids that come out of this, including OFDM-SRQCSK [36], OFDM-DCSK [37], and OFDM-OCVSK [38]. As an enhancement to the OFDM-DCSK system, a wavelet-packet-modulation-based DCSK (WPM-DCSK) system is introduced in [39]. This improvement is achieved by adopting a WPM system instead of an OFDM system. In [40], (PC-MC-M-CVCSK) a pre-coded-MC-M-ary-chaotic vector-cyclic shift keying system is introduced to enhance the system's BER through utilizing the concept of diagonalization to mitigate the noise and the interference signals.

In recent years, Index modulation is increasingly recognized as a promising technique in digital modulation in next-generation wireless communication systems [41]. By employing the indices of particular transmission entities, IM presents an opportunity to enhance energy efficiency and data rate while avoiding extra bandwidth or power consumption. Recent research efforts have explored the use of space, polarity, code, subcarrier (frequency), time slot, and the type of modulation as indices of modulation for improving the conveyance of additional information bits per modulation interval. [42, 43] propose innovative approaches that integrate code indices-modulation with differential chaos-shift- keying. The initial scheme integrates Walsh code indices modulation with SR-DCSK, whereas the subsequent scheme enhances CIM-DCSK through the implementation of noise reduction techniques and optimization of the power coefficient for reference and information-bearing signals. In [44] a new DCSK modulation method called CI-DCSK was introduced. It combined subcarrier index modulation with MC-DCSK to send more bits through the subcarrier's index, which sped up the transmission bit rate. A novel carrier-index modulation system (2CI-DCSK) was proposed in [45], designed to boost the transmitted data rate and bandwidth competence of CI-DCSK by splitting the data bit into two sub-blocks, with a single active subcarrier chosen from all other subcarriers based on the bits of index to transmit the DCSK bit. Modulated by a chaotic sequence in the first group and its Hilbert transform in the second group. (PI-DCSK) system is explored in [46] to enhance the bandwidth efficiency, energy efficiency,

and bit rate compared to rival scheme by transmitting the modulated bit through a permutated copy of the chaotic sequence, while the index modulation bits are utilized to choose predetermined permutations of the reference sequence. Code Index Modulation CIM integrates with (GCS-DCSK) and (MCS-DCSK) to present novel DCSK modulation schemes, namely (CIM-CS-DCSK) and (CIM-MCS-DCSK), as identified in [47, 48]. Both schemes employ a natural number k-combinatorial mapping method to choose Walsh codes with specified indices based on additional bits.

Dual index modulation used with pulse-position modulation-DCSK (PPM-DCSK) employs time resources to introduce the DCSK-DIM scheme in [49], wherein the frame bits are divided into dual orthogonal arms corresponding to the quadrature and in-phase arms. Subsequently, the bits of mapping from the quadrature and in-phase arms are converted into a couple of identifiable symbols, thereby optimizing the utilization of time resources. With the aim of raising the bit rate and boosting system's BER performance, a new M-ary DCSK modulation scheme was proposed in [50]. This scheme uses joint carrier-code index modulation to send more index bits, along with the M-ary DCSK modulated bit that are carried by the selected codes and active carriers. The disadvantage of this system is high complexity and low energy efficiency and spectral efficiency compared with rival systems. To accomplish a high and adjustable transmission bit rate, besides better energy efficiency and bandwidth efficiency for CI-DCSK, a high transmission rate solution, the CI-DCSK modulation scheme was introduced in [51]. In [52], two schemes are proposed called Grouping-subcarriers with index modulation-based DCSK: (GSIM-DCSKI, GSIM-DCSKII), the frame are split into L sub-block according to subcarriers in each scheme. The information bits in each sub-block are divided into carrier index bits and DCSK-modulated bits. One out of the total carriers is used to transmit the reference wavelet. Moreover, for each group of the subcarriers in GSIM-DCSKI, the index bits are utilized to choose the active subcarrier that carries the DCSK' bit, while in the GSIM-DCSK-II scheme, the index bits are employed to select the idle subcarrier and remain subcarriers used to convey the DCSK-modulated bits. In contrast to conventional CI-DCSK systems, both schemes offer improved energy efficiency and bit rates. (GCI-DM-DCSK-FM) modulation in [53] used the active and idle subcarriers for transmitting DCSK signals and QCSK signals, respectively. superior BER performance and greater transmission bit rate can be achieved by using the efficient full mapping method. Additionally, in order to improve the bit error rate behavior of the GCI-DM-DCSK-FM scheme, a noise reduction approach is utilized. The (JTFIM-MM-DCSK) scheme has been presented in [54] to accomplish a greater bit rate through the use of two prominent signal modes. One mode is used selected subcarriers in the modulation, and the other mode is employed unselected subcarriers. Besides the physical modulated bits, the time and carrier index bits are transmitted based on the situation of whether the time slots and subcarriers are active or not. In [55], the JTCDWT-DMIM-DCSK system was proposed as a dual index modulation scheme designed to obtain high data rates and spectral efficiency through the utilization of W discrete transforms and joint mapping for time slots to send additional bits, wherein chaotic sequences and their orthogonal copy generated from Hilbert transforms are transmitted separately during unselected and selected time slots. In addition to enhancing bit error rate (BER) and data rate performance, discrete W vectors are employed to broaden the transmitted bits. The indices of these vectors include extra bits. To further enhance BER performance, noise cancellation method is employed.

In the recent years, a new index modulation-aided DCSK, referred to as CTIM-DCSK in [56], this scheme is used with the frequency and time slot resources to accomplish a high transmission bit rate and used noise cancelation to enhance the system's performance regarding BER, but the system's complexity is still quite high. GFTIM-DCSK (grouping-frequency-time index modulation-based DCSK) was described with two versions in [57] and [58], these schemes improve the energy and bandwidth effectiveness of the (GSTIM-DCSK) system in furtherance of improving the data rate. In both schemes, the symbol bits are divided into L sub-blocks, just like in (GSTIM-DCSK). Time slot and subcarrier index bits in the first scheme were used to select the time slot and an active subcarrier, respectively, to transmit one DCSK modulated bit. In the second scheme, on the other hand, the index bits were used to select an inactive subcarrier and inactive time slot, and all of the extant time slots and subcarriers were used to transmit DCSK's bits. Therefore, GFTIM-DCSK-II has a higher bandwidth efficiency and transmission bit rate than GFTIM-DCSK-I, but a lower energy efficiency. New GSIM-DCSK systems, GSPIM-DCSKI and GSPIM-DCSK-II, with PI (permutation index modulation) are presented in [59]. Energy efficiency, data rate, and spectrum efficiency are the targets of these schemes. To guarantee that the basis is semi-orthogonal, the chaotic signal's length (the spreading factor) is long

in this system. Consequently, more process time is required.

Even though the advancements in dual index modulation aided DCSK discussed in the preceding research, the necessity for a DCSK system that satisfies contemporary wireless communication demands is imperative; this system must have a high transmitted data rate alongside substantial spectral and energy efficiency, all while maintaining reasonable complexity.

Inspired by these motivations, we suggest the Generalized Joint Subcarrier-time index modulation DCSK (GJSTIM-DCSK) scheme. (GJSTIM-DCSK) system aims to improve the transmission bit rate and the bandwidth effectiveness of the current dual index modulation–DCSK systems through using a grouping approach besides the K- compenatorial Mapping to choose active subcarriers and time slots based on index bits. Additionally, the proposed scheme employed orthogonal sinusoidal carriers for transmitting both the reference sequence and the modulated information signals. The contributions to this endeavor are delineated as follows:

1. A novel two-dimensional index modulation DCSK system labelled (GJSTIM-DCSK) is proposed. This system employed the frequency and the time indices to transmit more information bits, the index of these resources was selected using K-Mapping according to the index bits. Furthermore, the symbol bits are split equally among G groups; each group consists of modulated bits and index bits, where modulated bits are sent by all time slots of selected subcarriers and by unselected time slots of inactive subcarriers.
2. This study analyzes the energy and bandwidth efficiency, together with the system complexity, of the proposed system, comparing the findings with dual-index modulation DCSK schemes, including CTIM-DCSK, GFTIM-DCSK-II, and GSPIM-DCSK-II modulation systems, and traditional DCSK systems. The findings indicate that the GJSTIM-DCSK system has significantly enhanced data rates and spectrum efficiency.
3. The BER (bit error rate) analysis of the suggested scheme is also derived while evaluating the impact of multipath Rayleigh fading and AWGN channels. The suggested system's analysis is validated by comparing the simulation and theoretical results to those of conventional index modulation DCSK systems.

The subsequent parts of this work are organized in this way: part 2 defines the structure of the suggested GJSTIM-DCSK system. part 3 presents an analysis and comparison of transmission data rate and bandwidth efficiency. part 4 subsequently introduces the derived BER theory for the GJSTIM-DCSK modulation under multipath Rayleigh fading and Additive-White-Gaussian-Noise (AWGN) channels. Part 5 presents a comprehensive array of simulation data to validate the superior performance of our system. part 6 presents the analysis and comparison of the complexity. The final concluding remarks are provided in part 7.

2. GJSTIM-DCSK's model

2.1 Transmitter

The system's transmitter block diagram is clarified in Fig. 1. Employing a second-order Chebyshev polynomial function, the beginning phase includes the generation of a chaotic signal with θ length, which is rpresented by $\boldsymbol{C}_x = [C_{\mathrm{x},1}, C_{\mathrm{x},2},\ldots, C_{x,\theta}]$. The chaotic signal is normalized in order to achieve mean value of zero and mean squared value of unity, meaning that $E[\boldsymbol{C}_x]= 0$ and $E[\boldsymbol{C}_x^2] =1$. This function is defined as $C_{n+1} = 1\text{-}C_n^2$, where (n=1, 2, ….). A Hilbert transform can be used to generate the orthogonal chaotic signal $\boldsymbol{C}_y = [\, C_{\mathrm{y},1}\,,\ C_{y,2}\ ,\ldots,\ C_{y,\theta}\ ]$ from $\boldsymbol{C}_x$, which satisfies $\sum_{k=1}^{\theta} C_{x,k}C_{y,k} = 0$. In this system, there are 2^q+1 subcarriers, where q is an integer number, and $q \geq x_s$. Among them; one is reserved to carry $\boldsymbol{C}_x$ reference chaotic signal, and the rest 2^q subcarriers split equally to G sub-blocks each of them consists of N_S subcarriers, and N_C denotes the chosen subcarrier's number, M_S indicates overall time slots number, and M_C denotes the number of selected time slots. In particular, the GJSTIM-DCSK's frame is partitioned into G sub-blocks, every part has X bits expressed as

$$X = x_s + (N_s - N_c)x_t + N_cM_s + (N_s - N_c)(M_s - M_c) \quad (1)$$

These bits consist of $x_s = \left\lfloor log_2 \binom{N_S}{N_C} \right\rfloor$ bits are denoted as subcarrier index bits that are utilized to select $\mathrm{N_C}$ from $\mathrm{N_S}$ total subcarriers, and $(\mathrm{N_s}-\mathrm{N_c})\ \mathrm{x_t}$ bits, where $x_t = \left\lfloor log_2 \binom{M_S}{M_c} \right\rfloor$ bits are denoted as a time slot index bits which are utilized to select $\mathrm{M_C}$ time slots out of $\mathrm{M_S}$ total time slots on $(\mathrm{N_S} - \mathrm{N_C})$ inactive subcarriers, where $\binom{\cdot}{\cdot}$ represents binominal coefficient and $\lfloor\cdot\rfloor$ denotes floor function. Besides $N_cM_s + (N_s - N_c)(M_s - M_c)$DCSK modulated bits, first N_cM_s bits of them are transmitted by utilizing each time slot on active subcarriers, and the last

Received: December 18, 2024. Revised: January 12, 2025.

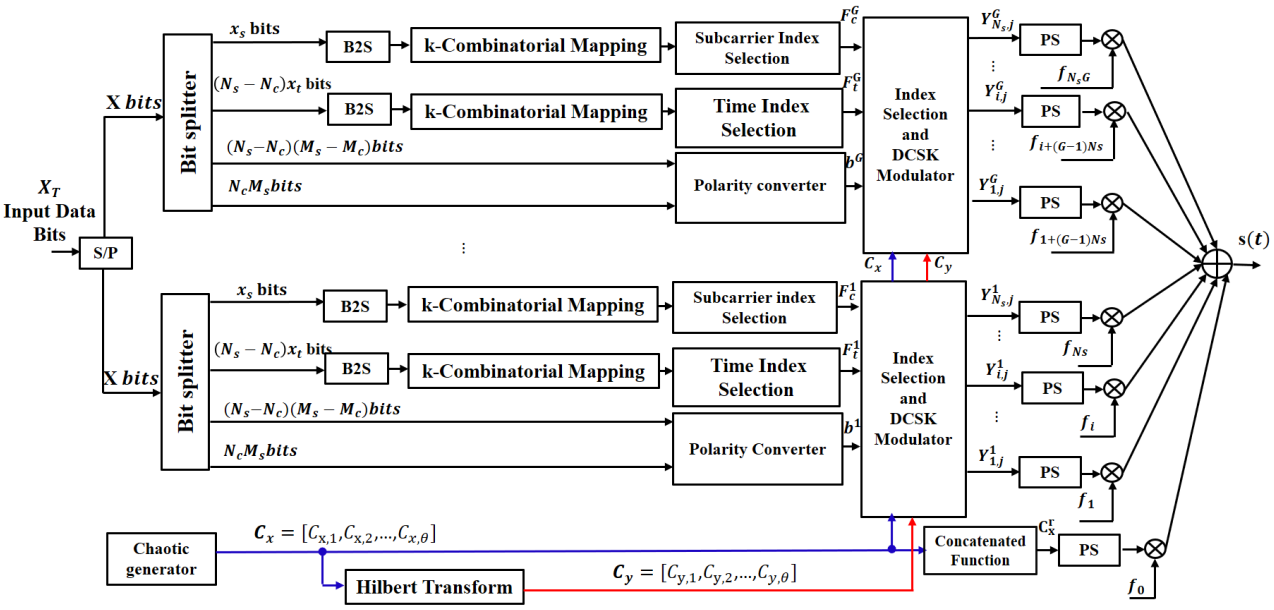

Figure. 1 GJSTIM-DCSK's transmitter block diagram

$(N_s - N_c)(M_s - M_c)$ bits are transmitted using unselected time slots on inactive subcarriers. Thus, the total transmitted bits of the GJSTIM-DCSK symbol are $X_T = GX$, where G is the sub-block's number in the system and denoted as $G = 2^q / N_s$.

In [60], k-combinatorial method was introduced, Employing a fixed number n and k, it establishes a one-to-one correspondence between natural numbers and k-combinations. It converts a natural number into a strictly decreasing series F=$\{\sigma_k, \ldots., \sigma_1\}$, where $\sigma_k > \cdots > \sigma_1 \geq 0$, which selects an element from the set $\{0, \ldots., n-1\}$ based on the following formula:

$$Z = \binom{\sigma_k}{k} + \cdots + \binom{\sigma_1}{2} + \binom{\sigma_1}{1}, \quad (2)$$

where $Z \in \left[0, \binom{n}{k} - 1\right]$. In GJSTIM-DCSK system for v^{th} frame and g^{th} group, where g ∈ {1, 2,...G}, the x_s bits are converted to a symbol through the operation of binary to decimal conversion, then directed to the k-Combinatorial mapping, which transforms this symbol to a vector of active subcarriers indices which are denoted as $F_c^g = [f_{c,1}^g, \ldots, f_{c,k}^g, \ldots f_{c,N_C}^g]$, for $0 < g \leq G$, where $f_{c,k}^g \in \{1,\ldots,N_S\}$, k = 1,..., N_C, and $f_{c,k1}^g \neq f_{c,k2}^g$ if $k1 \neq k2$. The mentioned above mapping method is applied to determine the selected time slots indices in ($N_s - N_c$) inactive subcarrier denoted as $F_t^g = [f_{t,1}^g, \ldots, f_{t,r}^g, \ldots, f_{t,(N_s-N_c)}^g]$, for $0 < g \leq G$, r =1,…,$(N_s - N_c)$,where $f_{t,r}^g$ is vector of M_c length and $f_{t,r}^g \in \{1,\ldots, M_S\}$. Subsequently, to extract unselected time slot, the complement of selected time slots $f_{t,r}^g$ are taken on the set $\{1,2,\ldots, M_s\}$is represented as $\widetilde{f_{t,r}^g} = C_{1:M_s} f_{t,r}^g$,where $C_a b$ determine the complement of subset b in set a. For more specifically, Table 1 illustrates an example of mapping method and selection of the subcarriers indices according to x_s sub carriers index bits for g^{th} group, N_s, N_c, x_s, x_t, $(N_s - N_c)x_t$, M_s, and M_c parameters are set to 4, 2, 2, 2, 4, 4, 2, respectively. According to x_s bits, there are $2^{x_s} = 4$ sets of subcarrier's indices takes from 6 sets in k-mapping as $\binom{N_s}{N_c} = 6$, each set consist of N_c of subcarrier indices,

Table 1. An example illustrates the selection of the 2 active subcarriers out of 4; according to 2 subcarriers index bits through K-combinatorial mapping for the g^{th} group

Sub-carrier index bits $x_s = 2$	Bit to symbol +1	Selected subcarrier indices F_c^g	k-combinatorial mapping 4 sets T_s	
			symbol	Subcarrier indices
[0 0]	1	{1,2}	1	{1, 2}
[1 1]	4	{1,4}	2	{1, 3}
[0 1]	2	{1,3}	3	{2, 3}
[1 0]	3	{2,3}	4	{1, 4}

 DOI: 10.22266/ijies2025.0331.26

Table 2. An example illustrates the selection of the 2 active time slots out of 4 time slots for each inactive subcarriers through k-combinatorial mapping for the g^{th} group

Time slot index bits	Bit to symbol+ 1 For Each row	Selected time slots indices F_t^g	k-combinatorial mapping 4 sets T_t	
			symbol	Time slots indices
[0 0 1 0] $\rightarrow \begin{bmatrix}0 & 0\\ 1 & 0\end{bmatrix}$	$\begin{bmatrix}1\\3\end{bmatrix}$	$\begin{bmatrix}\{1,2\}\\\{2,3\}\end{bmatrix}$	1	{1, 2}
[0 1 1 1] $\rightarrow \begin{bmatrix}0 & 1\\ 1 & 1\end{bmatrix}$	$\begin{bmatrix}2\\4\end{bmatrix}$	$\begin{bmatrix}\{1,3\}\\\{1,4\}\end{bmatrix}$	2	{1, 3}
[1 0 0 0] $\rightarrow \begin{bmatrix}1 & 0\\ 0 & 0\end{bmatrix}$	$\begin{bmatrix}3\\1\end{bmatrix}$	$\begin{bmatrix}\{2,3\}\\\{1,2\}\end{bmatrix}$	3	{2, 3}
[1 1 1 1] $\rightarrow \begin{bmatrix}1 & 1\\ 1 & 1\end{bmatrix}$	$\begin{bmatrix}4\\4\end{bmatrix}$	$\begin{bmatrix}\{1,4\}\\\{1,4\}\end{bmatrix}$	4	{1, 4}

and active subcarriers set chosen based on the symbol outputs from bit to symbol converter. For the same aforementioned example, Table 2 illustrates the k-combinatorial mapping to select the M_c active time slots for each inactive subcarrier based on $(N_s - N_c)x_t$ time slot index bits, also there are 2^{x_t} sets of time slots index in k –mapping to select active time slots from them.

Later, also for the g^{th} sub-block in the modulator, there are $N_c M_s$ modulated bits carrying by the reference signal $\boldsymbol{C}_x$ in an active subcarriers, and the last $(N_s - N_c)(M_s - M_c)$ bits are carried by the Hilbert transform chaotic signal $\boldsymbol{C}_y$ in an inactive subcarriers and unselected time slots, these modulated bits denoted as $b_{i,j} \in \{1, -1\}$ conveyed by i^{th} subcarrier and j^{th} time slot. Subsequently, the output of index selection and DCSK modulation block as in Fig.1 for the g^{th} Sub-block can be formulated as

$$Y_{i,j}^{g} = \begin{cases} b_{i,j}^{\mathrm{g}} C_{x,k} \ , for\ i \in F_c^{\mathrm{g}}, j = 1,2,..,M_s \\ 0 \quad , i \notin F_c^{\mathrm{g}} \ , j \in F_t^{\mathrm{g}} \\ b_{i,j}^{\mathrm{g}} C_{x,k} \ , \ for\ i \notin F_c^{\mathrm{g}}, j \in \widetilde{F_t^{\mathrm{g}}} \end{cases} \quad (3)$$

Algorithm 1 represents a pseudo-code of the transmitter implementation to help with understanding the transmitter modulation process for the g^{th} sub-block. In this algorithm, $Y_{i,j}$ indicates the transmission sequence carried by the i^{th} subcarrier based on its status, active or inactive. When the i^{th} subcarrier is in an active state, the modulated bits $b_{i,j}$ are multiplied by the chaotic sequence C_x with length θ and transmitted in each j^{th} time slot of this subcarrier, where $j = 1, 2, \dots, M_s$. In an inactive subcarrier, the modulated bits $b_{i,j}$ are multiplied by the Hilbert transform chaotic sequence C_y with length θ and transmitted in the j^{th} unselected time slot. In other cases, the output $Y_{i,j}$ goes to zero.

Algorithm 1: Modulation Process

Input: N_s, N_c, M_s, M_c, C_x, C_y, F_c^{g}, $\widetilde{F_t^{\mathrm{g}}}$

```
For i = 1,2, ..., N_s do
    If i ∈ F_c^g then
        For j = 1,2, ..., M_s do
            Y_{i,j} = b_{i,j} C_x
        End
    Else
        For j = 1,2, ..., M_s do
            If j ∈ F̃_t^g then
                Y_{i,j} = b_{i,j} C_y
            Else
                Y_{i,j} = 0
            End
        End
    End
End
Output : Y
```

The format structure of the information signal for the suggested system is exemplified in Fig. 2, where the zeroth subcarrier contains the reference samples that is repeated M_s in each time slot. The rows colored by blue represent active sub-carriers and the rest are inactive. The time slot of the inactive subcarrier filled with zero indicates the selected time slot, while the time slots colored by pink are unselected. Lastly, the output of the concatenated function is represented as C_x^r ,where $C_x^r = \left[C_{x,1}^r, C_{x,2}^r, \dots, C_{x,\beta}^r\right]$ and β is spreading factor which equal to $M_s\theta$,the C_x^r enter to pulsing shaping (PS), which is utilized to produce the analog version of the repeated reference signal and the data carrier-signals, where $C_x^r(t) = \sum_{k=1}^{\beta} C_{x,k}^r h(t - kT_c)$ is analog reference signal and transmitted by subcarrier with f_0 center frequency , while $y_{i,j}^{\mathrm{g}}(t) = \sum_{k=1}^{\theta} Y_{i,j}^{\mathrm{g}}\, h(t - kT_c)$ denote to information signal after pulse shaping filter,since h(t) represents the square root raised cosine filter and T_c denotes the time per chip. The GJSTIM-DCSK transmitted signal for v^{th} frame can be described as

$$s(t) = C_x^r(t)\cos(2\pi f_0 t + \varphi_0) + \sum_{\mathrm{g}=1}^{G}\sum_{i=1}^{N_S}\sum_{j=1}^{M_s} y_{i,j}^{\mathrm{g}}(t)\cos\left(2\pi f_{(g-1)N_s+i} t + \varphi_{(g-1)N_s+i}\right), \quad (4)$$

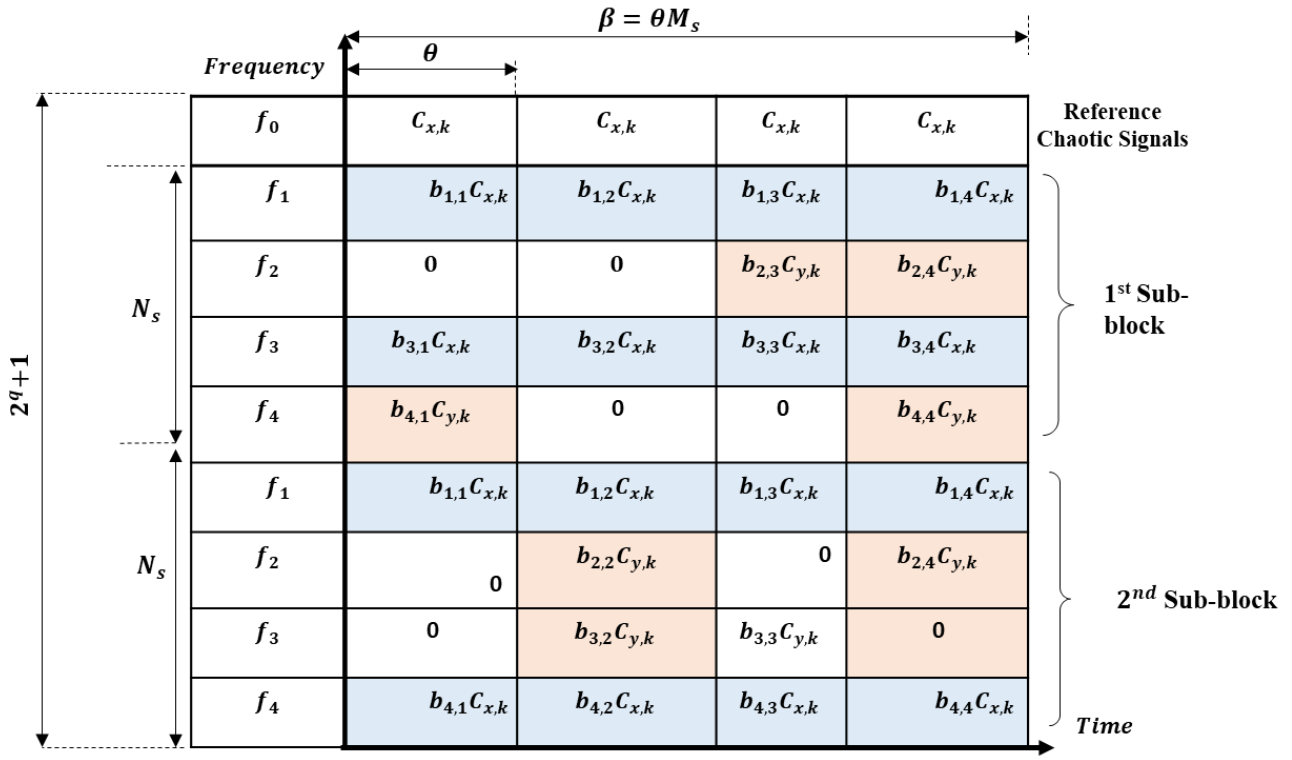

Figure. 2 The information sequence format for GJSTIM-DCSK scheme, where $N_S = 4, N_c = 2, M_s = 4, M_c = 2, G = 2$when active subcarriers indices for $1^{st}$and 2^{nd}Sub-block are {1,3} and { 1,4} respectively .While the selected time slot's indices on inactive subcarriers are {1,2},{2,3} for first Sub-block and {1,3},{1,4} for the 2^{nd} sub-block

The $\varphi_{(g-1)N_s+i}$ and $f_{(g-1)N_s+i}$ represent the phase angle and the center frequency of i^{th}subcarrier in the g^{th} sub-block, respectively, the subcarriers used in this system are orthogonal over the chip duration [30]. In general, the GJSTIM-DCSK's spreading factor can be described as $\beta = M_s\theta$.

2.2 Receiver

The GJSTIM- DCSK's receiver is illustrated in Fig. 3. The received wavelet is represented as:

$$r(t) = s(t) \otimes \sum_{l=1}^{L} \alpha_l \, \delta(t - \tau_l) + n(t), \quad (5)$$

where $\sum_{l=1}^{L} \alpha_l \, \delta(t - \tau_l)$is multipath Rayleigh fading channel model [57], L is the path number and τ_l , α_l, are the path delay and the channel coefficient of the l^{th}path, respectively, $\otimes$ represents the operator of convolution, and $n(t)$ refers to the Additive White Gaussian Noise signal where the mean is equal to zero and variance is equal to N0/2. The coefficients α_l are considered to be random variables where their distribution is an independent Rayleigh distribution. In the AWGN case, there is only one path and a single channel coefficient; in the Rayleigh fading case, there are at least two paths. Moreover, the $2^q + 1$orthogonal modulated carrier frequencies are used to initially separate the received signals. At each kT_c, the signals are sampled using the matched filters. These discrete outputs are stored in two matrices, The repeated chaotic signal is stored in matrix **A** which has dimension $1 \times \beta$ and information-bearing signal stored in matrix $\boldsymbol{B^g}$ for g^{th} sub-block with dimension $N_S \times \beta$. The reference signal matrix can be expressed as:

$$\boldsymbol{A} = [\, D_1^R, \cdots, \quad D_j^R, \cdots, \quad D_{M_s}^R], \quad (6)$$

and the matrix $\boldsymbol{B^g}$ can be expressed as:

$$\boldsymbol{B^g} = \begin{bmatrix} D_{1,1}^{I,g} & \cdots & D_{1,M_s}^{I,g} \\ \vdots & \ddots & \vdots \\ D_{N_s,1}^{I,g} & \cdots & D_{N_s,M_s}^{I,g} \end{bmatrix}, \quad (7)$$

where $D_j^R = [d_j^R(1), d_j^R(2), \ldots, d_j^R(\theta)]$, $j = 1, 2, \ldots, M_s$, and $D_{i,j}^{I,g} = [d_{i,j}^{I,g}(1), d_{i,j}^{I,g}(2), \ldots, d_{i,j}^{I,g}(\theta)]$, where $i = 1, 2, \ldots, N_s$, $j = 1, 2, \ldots, M_s$, $g = 1, 2, \ldots, G$, represents the sequences of received information that are situated in the g^{th}group, i^{th}subcarrier and j^{th} time slot. Afterwards, the average filter is applied to vector A over a window of length M_s. This process involves summing and averaging the values at corresponding locations in M_s segments of chaotic sequences with a length of θ. The result is

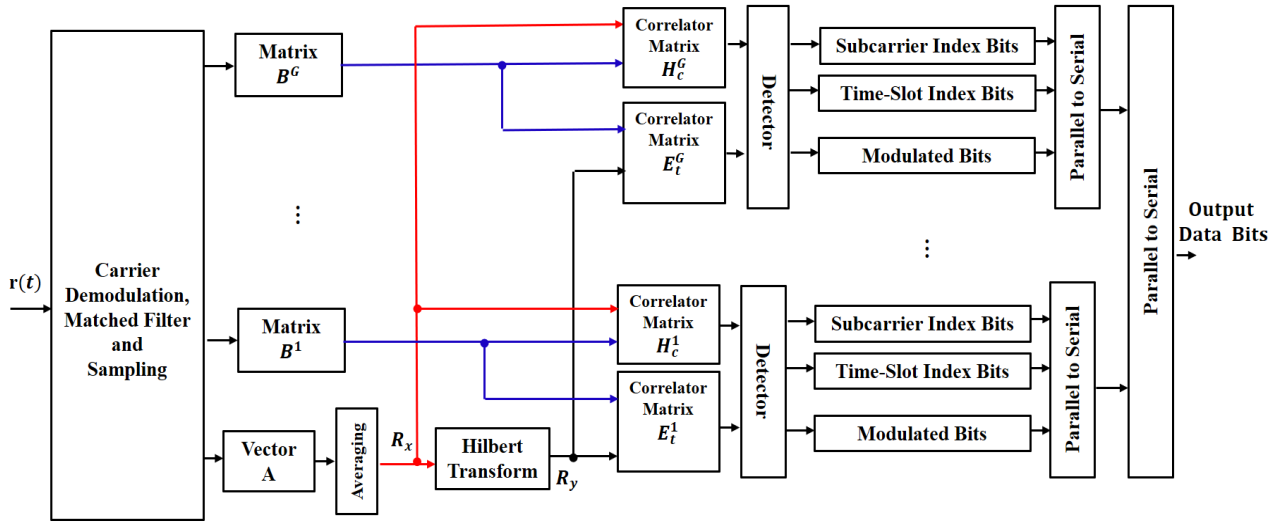

Figure. 3 The GJSTIM-DCSK's receiver Block diagram

$$R_x = \frac{1}{M_s}\sum_{i=1}^{M_s} D_i^R = \sum_{l=1}^{L} \alpha_l C_{x,\tau_l} + \widetilde{n_R}, \quad (8)$$

where, $\widetilde{n_R}$ represents AWGN corresponding to averaged chaos reference(R_x) with zero mean and variance of $N_0/2M_s$. Subsequently, the averaged received chaos reference R_x undergoes a Hilbert transform in order to produce an orthogonal vector of R_x denoted as R_y.

To recognize the indices of active subcarriers ζ_c^{g}, in the g^{th} group, we compute H_c^{g} correlator matrix through correlated averaged reference R_x with $\boldsymbol{B^{\mathrm{g}}}$,where $H_c^{\mathrm{g}} \in \mathbb{R}^{N_s \times M_s}$

$$H_c^{\mathrm{g}} = \begin{bmatrix} R_x(D_{1,1}^{I,\mathrm{g}})^T & \cdots & R_x(D_{1,M_s}^{I,\mathrm{g}})^T \\ \vdots & \ddots & \vdots \\ R_x(D_{N_s,1}^{I,\mathrm{g}})^T & \ldots & R_x(D_{N_s,M_s}^{I,\mathrm{g}})^T \end{bmatrix} \quad (9)$$

Algorithm 2 illustrates an active subcarriers index detection, which takes as inputs not only the produced matrix H_c^{g} but alsoN_s, N_c, T_c, x_s , Among the N_s variables the algorithm finds the top $N_c$maximum values and stores them in the vector ζ_c^{g}. Then, the vector ζ_c^{g} is sorted to get the vector that corresponds to itself. For the purpose of retrieving the remaining bits in inactive subcarriers, we find the complement of N_c to get the inactive subcarriers indices by complementing the element in ζ_c^{g} with element in the set {1,2,…, N_s }.And vector ζ_c^{g} converts to symbol S_C according to k- mapping denoted as T_s in Algorithm 2 to find $\widehat{x_s}$ active subcarrier index bits.

Algorithm 2: Active subcarrier index detection for the g^{th} group

Input:N_s,N_c, H_c^{g},T_c,x_s
For $i = 1,2,\ldots,N_s$ **do**
  $H_{max}(i) = \max\left(\left|H_c^{\mathrm{g}}(i,:)\right|\right)$
End
For j = 1,2, … , $\mathrm{N_c}$ **do**
  [~,r_s]=find{$|H_{max}|$==max($|H_{max}|$)}
    $H_{max}(r_s)$=0; $\zeta_c^{\mathrm{g}}(\mathrm{j}) = r_s$
End
$\zeta_c^{\mathrm{g}} = sort(\zeta_c^{\mathrm{g}})$; $\widetilde{\zeta_c^{\mathrm{g}}}$=complement($\zeta_c^{\mathrm{g}}$)
For k=1,2,..,$\mathbf{2^{x_s}}$ **do**
  If ζ_c^{g}= =T_s(k,:) **then**
    S_C =k
  End
End
S_C =S_C -1
$\widehat{x_s}$ =decimal to bit (S_C,x_s)
Output : ζ_c^{g}, $\widetilde{\zeta_c^{\mathrm{g}}}$, $\widehat{x_s}$

Once the active subcarriers have been found, the modulated bits can be figured out by looking at the real decision variable's sign in the active subcarriers rows of the matrix H_c^{g}. For example, '0' for less than zero and '1' for more than zero.

For each sub-block a matrix $\boldsymbol{E_t^{\mathrm{g}}} \in \mathbb{R}^{(N_s-N_c)\times M_s}$ is built for recovering the information bits on the inactive subcarriers. This is made by correlating the output of the Hilbert transform R_Y with $(N_s - N_c)$ rows of $\boldsymbol{B^{\mathrm{g}}}$ these rows have indices of inactive subcarriers in the vector $\widetilde{\zeta_c^{\mathrm{g}}}$,where $\widetilde{\zeta_c^{\mathrm{g}}}$ are the set of an inactive subcarrier indices of length $(N_s - N_c)$,

$$\boldsymbol{E_t^{\mathrm{g}}} = \begin{bmatrix} R_Y(D^{I,\mathrm{g}}_{\widetilde{\zeta_c^{\mathrm{g}}}(1),1})^T & \dots & R_Y(D^{I,\mathrm{g}}_{\widetilde{\zeta_c^{\mathrm{g}}}(1),M_s})^T \\ \vdots & \ddots & \vdots \\ R_Y(D^{I,\mathrm{g}}_{\widetilde{\zeta_c^{\mathrm{g}}}(N_s-N_c),1})^T & \dots & R_Y(D^{I,\mathrm{g}}_{\widetilde{\zeta_c^{\mathrm{g}}}(N_s-N_c),M_s})^T \end{bmatrix} \quad (10)$$

Algorithm 3 performs selected time slots detection using the matrix $\boldsymbol{E_t^{\mathrm{g}}}$ together with $\widetilde{\zeta_c^{\mathrm{g}}}$,N_s , N_c, M_s, M_c , T_t,and x_t as input, where T_t is time slots K-combinatorial mapping. Among the $M_s$variables in each row in matrix $\boldsymbol{E_t^{\mathrm{g}}}$ the algorithm finds the top $(M_s - M_c)$ maximum values and stores them in the matrix $\widetilde{\zeta_{tt}^{\mathrm{g}}} \in \mathbb{R}^{(N_s-N_c)\times(M_s-M_c)}$, this matrix consists of indices of unselected time slots.

Next, find the matrix ζ_{tt}^{g} from the complement of matrix $\widetilde{\zeta_{tt}^{\mathrm{g}}}$, which consist of selected time slot indices, subsequently, the algorithm mapping each row in ζ_{tt}^{g} to symbol S_t by invers operation of k-combinatorial mapping according to T_t map and convert the symbol to $\widehat{x_t}$ bits that represents the time slot index bits on the g^{th} sub-block and the same algorithm is applied for each sub-block.

Algorithm 3: Selected time slots detection for the g^{th} sub-block

Input: N_s,N_c, M_s, M_c, E_t^{g},x_t , T_t
For $i = 1, 2, \dots, N_s - N_c$ **do**
  K_m=E_t^{g}
  For j=1,2,$M_s - M_c$ **do**
    [~,r_s]= find{$|K_{m,max}|$==max($|K_m(i,:)|$)}
    $K_m(i,:) = 0$; $\widetilde{\zeta_t^{\mathrm{g}}} = r_s$
  End
  $\widetilde{\zeta_t^{\mathrm{g}}} = sort(\widetilde{\zeta_t^{\mathrm{g}}})$;
  $\widetilde{\zeta_{tt}^{\mathrm{g}}}(i,:) = \widetilde{\zeta_t^{\mathrm{g}}}$
  ζ_t^{g} =complement ($\widetilde{\zeta_t^{\mathrm{g}}}$)
  $\zeta_{tt}^{\mathrm{g}}(i,:)$ =ζ_t^{g}
  For $k = 1,2, N_s - N_c$ **do**
    If $\zeta_t^{\mathrm{g}} == T_t(k,:)$ $S_t = k$
    End
  End
  $S_t = S_t - 1$
  $\widehat{x_t}$ =decimal to bit (S_t,x_t)
End
Output : ζ_{tt}^{g}, $\widetilde{\zeta_{tt}^{\mathrm{g}}}$, $\widehat{x_t}$

Finally, the modulated information bits conveyed by inactive subcarriers and unselected time slots determined by looking at the sign of $(M_s - M_c)$ decision variables in each row of E_t^{g}, that are located in columns with indices equal to the indices of unselected time slots in $\widetilde{\zeta_{tt}^{\mathrm{g}}}$.

3. Transmission bits rate and bandwidth efficiency analysis

In this part, the transmission bit rate and bandwidth efficiency of the GJSTIM-DCSK system are computed, and the results are contrasted with those of other systems, for example the DCSK system, CI-DCSK, CTIM-DCSK, MC-DCSK, GSIM-DCSK-II, GFTIM-DCSK-II, and GSPIM-DCSK-II. The data rate in this analysis [56, 61] is derived from the proportion of total transmitted bits to the transmission time per symbol. Table 3 shows the comparison in bit rate and bandwidth efficiency between the GJSTIM-DCSK system and the others. The GJSTIM-DCSK system has data rate equal to $\frac{X_T}{\beta T_c}$, with βT_c transmission period. Moreover, the bits rate of the GFTIM-DCSK-II, GSPIM-DCSK-II, GSIM-DCSK-II, and CTIM-DCSK schemes can be defined as $\frac{X_{T1}}{\beta T_C}$, $\frac{X_{T2}}{\beta T_C}$, $\frac{X_{T3}}{\beta T_C}$, and $\frac{M_s X_{T4}}{(M_s+1)\beta T_c}$, respectively. Also, $X_{T1} = G[(N_s M_s \text{ -1})+\lfloor \log_2 N_s \rfloor +\lfloor \log_2 M_s \rfloor]$, $X_{T2} = G\left[\lfloor \log_2 N_s \rfloor +(N_s - 1)\left(\lfloor \log_2 N_p \rfloor + 1\right)\right]$, $X_{T3} = G[\lfloor \log_2 N_s \rfloor + N_s - 1]$ and $X_{T4} = \lfloor \log_2 N_s \rfloor + \lfloor \log_2 M_s \rfloor + (N_s - 1)(M_s - 1)$. As well as, the bits rate of remaining schemes are written in Table 3.The bits rate of the suggested GJSTIM-DCSK system is contrasted with its competitor system in Fig. 4, with the parameters set as follows: N_s=16, N_c=1, $M_c = 4$, G=2, and N_p=8. In this situation, $N_s$and M_s represent the subcarriers number and the time slots number, respectively. The activated subcarriers are indicated by N_c, and the selected time slots are represented by M_c. Besides that, the number of permutation chaotic operator of GSPIM-DCSK-II is represented by N_p. The same parameters are applied to the other systems for an equitable comparison. As the M_s number increases, it is apparent that the bits rate of the suggested GJSTIM-DCSK scheme surpasses that of the competing systems.

Also Fig. 5 shows another comparison of GJSTIM-DCSK's data rate versus the same system but with varying G, and the parameters set to the same values except M_s is set to 8. It is clear that the bits rate of the suggested scheme surpasses that of the rival schemes with increasing the sub-blocks number (G) Generally, the bandwidth efficiency defined as the bits rate to bandwidth ratio [52, 57, 62]. Table 3

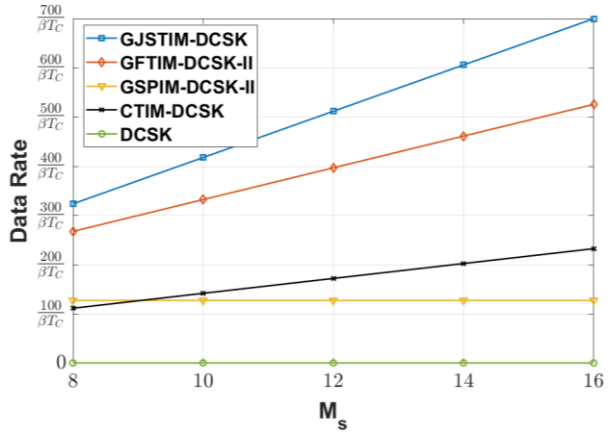

Figure. 4 Comparison of the GJSTIM-DCSK's data rate versus different DCSK modulations with varying M_s

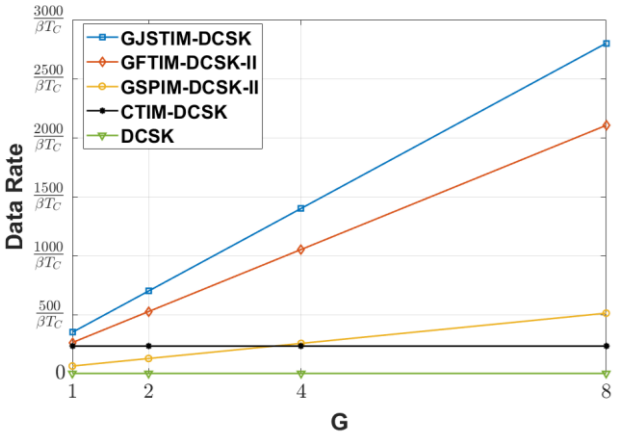

Figure. 5 Comparison of the GJSTIM-DCSK's data rate versus different DCSK modulations with varying G

Table 3. Transmission bits rate and bandwidth efficiency comparison between the GJSTIM-DCSK and the other DCSK modulation schemes

Scheme	bits Rate	Bandwidth efficiency
GJSTIM-DCSK	$\frac{X_T}{\beta T_C}$	$\frac{X_T}{(GN_S+1)\beta T_C w}$
GFTIM-DCSK_II [58]	$\frac{X_{T1}}{\beta T_C}$	$\frac{X_{T1}}{(GN_S+1)\beta T_C w}$
GSPIM_DCSK -II [59]	$\frac{X_{T2}}{\beta T_C}$	$\frac{X_{T2}}{(GN_S+1)\beta T_C w}$
GSIM_DCSK-II [52]	$\frac{X_{T3}}{\beta T_C}$	$\frac{X_{T3}}{(GN_S+1)\beta T_C w}$
CTIM_DCSK [56]	$\frac{M_s X_{T4}}{(M_s+1)\beta T_c}$	$\frac{M_s X_{T4}}{N_s(M_s+1)\beta T_c w}$
CI_DCSK[44]	$\frac{N_s-1+\log_2 N_s}{\beta T_c}$	$\frac{N_s-1+P1}{(N_s+1)\beta T_c w}$
MC-DCSK [30]	$\frac{N_S}{\beta T_C}$	$\frac{N_s}{(N_s+1)\beta T_C w}$
DCSK [7]	$\frac{1}{\beta T_C}$	$\frac{1}{\beta T_C w}$

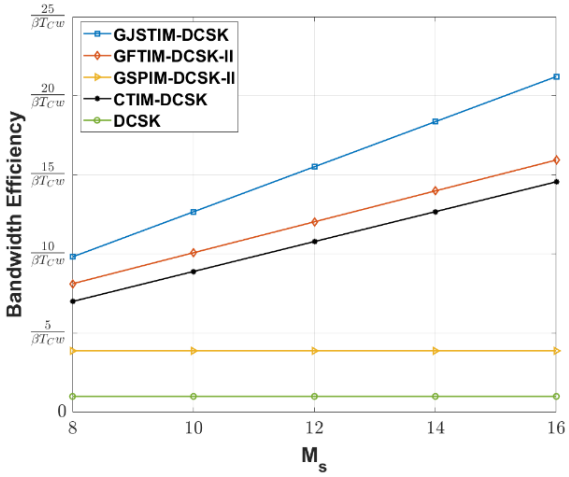

Figure. 6 Comparison of the GJSTIM-DCSK's bandwidth efficiency versus different DCSK modulations with varying M_s

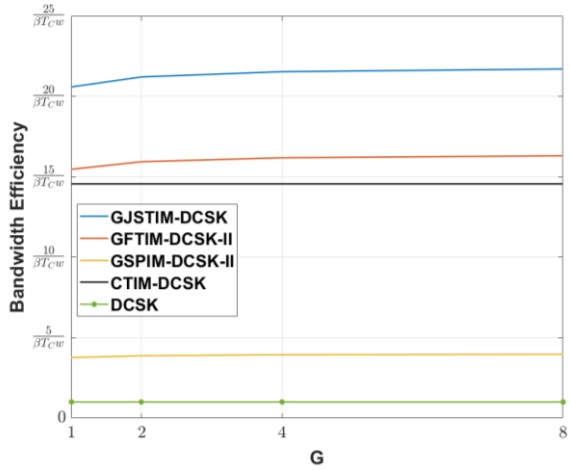

Figure. 7 Comparison of the GJSTIM-DCSK's bandwidth efficiency versus different DCSK modulations with varying G

explains a contrast of the bandwidth efficiency of the suggested system with various modulation schemes, with ω denoting the bandwidth of each subcarrier, under the assumption that the bandwidth is identical across each subcarrier. Fig. 6 illustrates the contrast of the GSTIM-DCSK's bandwidth efficiency versus different DCSK modulations with varyingM_s. This figure shows that an increasing in the time slots number leads to a significant enhancement in the bandwidth efficiency of the GJSTIM-DCSK modulation in comparison to other modulation schemes, and set up parameters as defined below: N_s=16, N_c=1, M_c = 4 G=2, and N_p=8. At M_s = 16, the bandwidth efficiency of the GJSTIM-DCSK system exceeds that of the GFTIM-DCSK-II by approximately 1.33 times and the CTIM-DCSK system by 1.45 times and is higher than that of GSPIM-DCSK-II by 5.5 times. As illustrated in Fig. 6, this enhancement is due to an increased number of

bits transmitted across additional time slots when operating within the identical bandwidth as other systems. Likewise, Fig. 7 indicates that an increase in the sub-blocks number(G) cause a significant boost in the bandwidth efficiency of the suggested scheme related to other modulation schemes, while the parameters are set as in Fig. 6, but M_s has a value equal to 8. At G=8, the GJSTIMG-DCSK system has a bandwidth efficiency that is around 1.33 times larger than that of the GFTIM-DCSK-II scheme and about 1.49 and 5.49 times more than that of the CTIM-DCSK and GSPIM-DCSK-II schemes, respectively.

4. BER (Bit Error Rate) performance analysis

The GJSTIM-DCSK receiver starts the bit recovery process through finding an active subcarrier. The modulated information bits are subsequently extracted from the active subcarriers. Afterwards, the receiver detects the time slot indices for the inactive subcarriers, facilitating the extraction of modulated bits from these subcarriers as well. There exist two different instances of the decision variable throughout the information bits' recovery process:

Case1: in this case there are three variable decisions in correlator matrix H_c^{g}, which are utilized to detect the indices of active subcarriers and recover the modulated bit conveyed by these active subcarriers as below:

1. The current time slot's information signal in active sub carriers

$$Z_1^i = \left[\sum_{l=1}^{L} \alpha_l \, C_x + \widetilde{n_R}\right]\left[\sum_{l=1}^{L} \alpha_l \, b_{i,j} C_x + n_I^{i,j}\right]^T, \quad (11)$$

where $\widetilde{n_R}$ is the average added AWGN corresponding to reference signal with mean is equal to zero and variance is equal to $\frac{N_0}{2M_s}$, and $n_I^{i,j}$ is AWGN added to information signal in i subcarrier and j time slot.

2. The unselected time slot's information signal in inactive sub carriers

$$Z_2^i = \left[\sum_{l=1}^{L} \alpha_l \, C_x + \widetilde{n_R}\right]\left[\sum_{l=1}^{L} \alpha_l \, b_{i,j} C_y + n_I^{i,j}\right]^T \quad (12)$$

3. The selected time slots in inactive subcarriers, which means that no bits are being sent

$$Z_3^i = \left[\sum_{l=1}^{L} \alpha_l \, C_x + \widetilde{n_R}\right] {n_I^{i,j}}^T \quad (13)$$

Case 2: In this case, we have two decision variables from the correlator matrix $\boldsymbol{E_t^{\mathrm{g}}}$ in the receiver used to detect the selected time slot indices, and followed by modulated bits recovery.

1. Unselected time slot's information signal modulated by C_y orthogonal reference signal of $\boldsymbol{E_t^{\mathrm{g}}}$.

$$Z_4^J = \left[\sum_{l=1}^{L} \alpha_l \, C_y + \widetilde{n_R}\right]\left[\sum_{l=1}^{L} \alpha_l \, b_{i,j} C_y + n_I^{i,j}\right]^T \quad (14)$$

2. The decision variables in selected time slots of $\boldsymbol{E_t^{\mathrm{g}}}$, which don't have any conveyed information.

$$Z_5^J = \left[\sum_{l=1}^{L} \alpha_l \, C_y + \widetilde{n_R}\right] {n_I^{i,j}}^T \quad (15)$$

In This Paper, the Gaussian approximation (GA) method is applied to evaluate the BER of the proposed system, which supposes a constant transmitted bit energy, E_b [15]. This method also demonstrates that, given a sufficiently big spreading factor, the system's decision variable belongs to a Gaussian distribution. Consequently, for a large β, the random variables $Z_1^i, Z_2^i, Z_3^i, Z_4^j$ and Z_5^j follow Gaussian distributions [1]. Let E_b is the bit energy in the proposed system GJSTIM-DCSK which is expressed as $E_b = \frac{X_t(C_x {C_x}^T)}{X_T}$, where $X_t = G\begin{pmatrix} N_c M_s + \\ (N_s - N_c)(M_s - M_c) \end{pmatrix} + M_s$, and assuming $b_{i,j} = 1$. Then, the mean value and variance of these variables may be calculated in terms of E_b as below:

$$E\left[Z_1^i\right] = \sum_{l=1}^{L} {\alpha_l}^2 \frac{E_b X_T}{X_t} = \mu_1 \quad (16)$$

$$var\left[Z_1^i\right] = \sum_{l=1}^{L} {\alpha_l}^2 \frac{E_b X_T}{X_t} \frac{N_0}{2}\left(1 + \frac{1}{M_s}\right) + \theta \frac{{N_0}^2}{4M_s} = \sigma_1^2 \quad (17)$$

Additionally, based on Eqs. (12) and (13), we can determine the mean value and variance of Z_2^i and Z_3^i in the following manner:

$$E\left[Z_2^i\right] = 0 = \mu_2, \quad (18)$$

where $E\left[C_x C_y^T\right] = 0$, result of the orthogonality, and the energy of them assumed identical.

$$var\left[Z_2^i\right] = \sum_{l=1}^{L} {\alpha_l}^2 \frac{E_b X_T}{X_t} \frac{N_0}{2}\left(1 + \frac{1}{M_s}\right) + \theta \frac{N_0^2}{4M_s} = \sigma_2^2 \quad (19)$$

$$E\left[Z_3^i\right] = 0 = \mu_3 \quad (20)$$

$$var\left[Z_3^i\right] = \sum_{l=1}^{L} {\alpha_l}^2 \frac{E_b X_T}{X_t}\frac{N_0}{2} + \theta\frac{N_0^2}{4M_s} = \sigma_3^2 \quad (21)$$

From Eqs. (14) and (15), the mean value and variance of variables Z_4^J and Z_5^j are calculated as follows:

$$E\left[Z_4^J\right] = \sum_{l=1}^{L} {\alpha_l}^2 E[C_x C_x^T] = \sum_{l=1}^{L} {\alpha_l}^2 \frac{E_b X_T}{X_t} = \mu_4 = \mu_1 \quad (22)$$

Since C_x and C_y have the same energy as mentioned previously, then

$$var\left[Z_4^J\right] = \sum_{l=1}^{L} {\alpha_l}^2 \frac{E_b X_T}{X_t}\frac{N_0}{2}\left(1+\frac{1}{M_s}\right) + \theta\frac{{N_0}^2}{4M_s} = \sigma_4^2 = \sigma_1^2 \quad (23)$$

$$E\left[\, Z_5^j\right] = 0 = \mu_5 = \mu_3 \quad (24)$$

$$var\left[Z_5^j\right] = \sigma_5^2 = \sigma_3^2 \quad (25)$$

4.1 Error rate probability of subcarrier index detection, P_e^{sd}

The decision variable for the initially timeslot of each subcarrier is selected for recovery throughout the subcarrier index detection process. Consequently, a total of N_s decision variables are involved in the process. The magnitude of the decision variables in selected time slots and in inactive subcarriers and the variables in unselected time slots and in inactive subcarriers is denoted as $|Z_{3,u}^i|$and $|Z_{2,v}^i|$ respectively, where $u = 1, \dots, M_c$ and $v = 1, \dots, M_s - M_c$.

Let defined $Y = min\{|Z_{1,w}^i|\}$, since $w = 1, \dots, N_c$ and $X_1 = max\{|Z_{2,v}^i|\}$, $X_2 = max\{|Z_{3,u}^i|\}$. Then the error probability of index detection is denoted as [26, 62]

$$P_e^{sd} = \int_0^\infty \Big(\big(1 - P_r(X_1 \le y)\big)\big(1 - P_r(X_2 \le y)\big)\Big) f_Y(y)\, dy$$

$$P_e^{sd} = \int_0^\infty \left[\left[1 - \left(F_{|Z_{2,v}^i|}(y)\right)^{N_s - N_c}\right]\left[1 - \left(F_{|Z_{3,u}^i|}(y)\right)^{N_s - N_c}\right]\right] f_Y(y)\, dy \quad (26)$$

where $F_{|Z_{2,v}^i|}$ and $F_{|Z_{3,u}^i|}$ are denote CDF (the cumulative distribution function) of $|Z_{2,v}^i|$ and $|Z_{3,u}^i|$ respectively .As the N_c random variables from $\{|Z_{1,2}^i|, |Z_{1,2}^i|, \cdots, |Z_{1,N_c}^i|\}$ are independent of one another, the CDF of Y is described as

$$F_Y(y) = 1 - \left[1 - F_{|Z_{1,w}^i|}(y)\right]^{N_c} \quad (27)$$

The PDF (probability density function) of Y can be derived from $F_Y(y)$, which is as described below:

$$f_Y(y) = N_c\left[1 - F_{|Z_{1,w}^i|}(y)\right]^{N_c - 1} f_{|Z_{1,w}^i|}(y) \quad (28)$$

So, the error probability of subcarrier index detection in Eqs. (26) may be further computed as

$$P_e^{sd} = \int_0^\infty N_c \left[\left[1 - \left(F_{|Z_{2,v}^i|}(y)\right)^{N_s - N_c}\right]\left[1 - \left(F_{|Z_{3,u}^i|}(y)\right)^{N_s - N_c}\right]\right]\left[1 - F_{|Z_{1,w}^i|}(y)\right]^{N_c - 1} f_{|Z_{1,w}^i|}(y)\, dy \quad (29)$$

Where $|Z_{1,w}^i|$, $|Z_{2,v}^i|$ and $|\, Z_{3,u}^i\,|$ are random variables, which are follow folded normal distribution, and $F_{|Z_{1,w}^i|}(y)$, $F_{|Z_{2,v}^i|}(y)$ and $F_{|Z_{3,u}^i|}(y)$ denote CDF of these variables respectively. While $f_{|Z_{1,w}^i|}(y)$ represent PDF of $|Z_{1,w}^i|$ .So $F_{|Z_{1,w}^i|}(y)$, $F_{|Z_{2,v}^i|}(y)$, $F_{|Z_{3,u}^i|}(y)$ and $f_{|Z_{1,w}^i|}(y)$ can be expressed as [57], [62],[63]:

$$F_{|Z_{1,w}^i|}(y) = \frac{1}{2}\left[erf\left(\frac{y-\mu_1}{\sqrt{2\sigma_1^2}}\right) + erf\left(\frac{y+\mu_1}{\sqrt{2\sigma_1^2}}\right)\right] = \Xi(y; \mu_1, \sigma_1^2) \quad (30)$$

$$F_{|Z_{2,v}^i|}(y) = \Xi(y; \mu_2, \sigma_2^2) = erf\left(\frac{y-\mu_2}{\sqrt{2\sigma_2^2}}\right) \quad (31)$$

$$F_{|Z_{3,u}^i|}(y) = \Xi(y; \mu_3, \sigma_3^2) = erf\left(\frac{y-\mu_3}{\sqrt{2\sigma_3^2}}\right) \quad (32)$$

$$f_{|Z_{1,w}^i|}(y) = \frac{1}{\sqrt{2\pi\sigma_1^2}}\left[e^{\frac{-(y-\mu_1)^2}{2\sigma_1^2}} + e^{\frac{-(y+\mu_1)^2}{2\sigma_1^2}}\right] = \lambda(y; \mu_1, \sigma_1^2) \quad (33)$$

The final formula of carrier index detection can be calculated as (34), according to Eqs. (29) to (33).

$$P_e^{sd} = \frac{1}{\sqrt{2\pi\sigma_1^2}} \int_0^{\infty} N_c \times \left[\left[1 - \left(erf\left(\frac{y-\mu_2}{\sqrt{2\sigma_2^2}}\right)\right)^{N_s-N_c}\right]\left[1 - \left(erf\left(\frac{y-\mu_3}{\sqrt{2\sigma_3^2}}\right)\right)^{N_s-N_c}\right]\right]\left[1 - \frac{1}{2}\left[erf\left(\frac{y-\mu_1}{\sqrt{2\sigma_1^2}}\right) + erf\left(\frac{y+\mu_1}{\sqrt{2\sigma_1^2}}\right)\right]\right]^{N_c-1}\left[e^{\frac{-(y-\mu_1)^2}{2\sigma_1^2}} + e^{\frac{-(y+\mu_1)^2}{2\sigma_1^2}}\right]dy \quad (34)$$

$$P_e^{td} = \frac{1}{\sqrt{2\pi\sigma_4^2}} \int_0^{\infty}\left[1 - \left(erf\left(\frac{y-\mu_5}{\sqrt{2\sigma_5^2}}\right)\right)^{M_c}\right](M_s - M_c)\left[1 - \left[\frac{1}{2}\left[erf\left(\frac{y-\mu_4}{\sqrt{2\sigma_4^2}}\right) + erf\left(\frac{y+\mu_4}{\sqrt{2\sigma_4^2}}\right)\right]\right]\right]^{M_s-M_c-1}\left[e^{\frac{-(y-\mu_4)^2}{2\sigma_4^2}} + e^{\frac{-(y+\mu_4)^2}{2\sigma_4^2}}\right]dy \quad (39)$$

4.2 Error rate probability of time-slot index detection P_e^{td}

The time slot's index bits on inactive subcarriers are recoverable once the indices of active subcarriers are detected. This process involves M_s decision variables on inactive subcarriers, represented by $Z_{4,m}^j$ and $Z_{5,n}^j$, which denote the decision variables in unselected time slots and the decision variable in selected time slots respectively, where $m = 1, 2, \ldots, M_s - M_c$ and $n = 1, 2, \ldots, M_c$. Hence, we describe $\Gamma = \min\{|Z_{4,m}^j|\}$ and $\Upsilon = max\{|Z_{5,n}^j|\}$, It is evident that the time slot mapping bits demodulation can precisely recover when Υ value is smaller than Γ.

Then the erroneous index detection probability Pe^{Td} is denoted as[49, 62]

$$P_e^{td} = 1 - P_r\{\Upsilon < \Gamma\} = \int_0^{\infty}\left[1 - \left(F_{|Z_{5,n}^j|}(y)\right)^{M_c}\right](M_s - M_c)\left[1 - F_{|Z_{4,m}^j|}(y)\right]^{M_s-M_c-1} f_{|Z_{4,m}^j|}(y)\, dy \quad (35)$$

where

$$F_{|Z_{5,n}^j|}(y) = \Xi\left(y; \mu_5, \sigma_5^2\right) = erf\left(\frac{y-\mu_5}{\sqrt{2\sigma_5^2}}\right) \quad (36)$$

$$F_{|Z_{4,m}^j|}(y) = \Xi(y; \mu_4, \sigma_4^2) = \frac{1}{2}\left[erf\left(\frac{y-\mu_4}{\sqrt{2\sigma_4^2}}\right) + erf\left(\frac{y+\mu_4}{\sqrt{2\sigma_4^2}}\right)\right], \quad (37)$$

and

$$f_{|Z_{4,m}^j|}(y) = \lambda(y; \mu_4, \sigma_4^2) = \frac{1}{\sqrt{2\pi\sigma_4^2}}\left[e^{\frac{-(y-\mu_4)^2}{2\sigma_4^2}} + e^{\frac{-(y+\mu_4)^2}{2\sigma_4^2}}\right] \quad (38)$$

Furthermore, the error probability for the time slot detection is calculated as (39) through substituting Eqs. (36), (37), and (38) into (39).

4.3 Error rate probability of modulated bits P_e^{md}

When detecting the carrier and time slot indices correctly, modulated bits are demodulated on each time slots of active subcarriers and on unselected time slots of inactive subcarriers. Based on the previously obtained mean in Eqs. (16), (22) and variance in Eqs. (17) and (23) of the decision variables $Z_{1,w}^i$ and $Z_{4,m}^j$, since it's $\mu_1 = \mu_4$, and $\sigma_1^2 = \sigma_4^2$, therefore the error probability of DCSK bits is equally and is expressed as:

$$P_e^{md} = 0.5erf\left(\left(\frac{2\sigma_1^2}{{\mu_1}^2}\right)^{-0.5} \right)$$
$$= 0.5erf\left(\left(\frac{2(M_s+1)X_t}{M_s\gamma_b X_T} + \frac{\theta {X_t}^2}{2{\gamma_b}^2 {X_T}^2 M_s}\right)^{-0.5} \right), \quad (40)$$

where $\gamma_b = \sum_{l=1}^{L} {\alpha_l}^2 \frac{E_b}{N_0}$.

4.4 GJSTIM-DCSK's BER

The bit error rate probability of the subcarrier index bits is given by P_{sa}, the time slot index bits is given by P_{ta}, and the bit error rate probability of the information modulated bits transmitted by all time slots of active subcarriers and modulated bits transmitted by unselected time slots of inactive subcarriers are represented as P_m^1 and P_m^2, respectively. Thus, the GJSTIM-DCSK's BER is expressed as

$$BER_{GJSTIM-DCSK} = \frac{1}{X_T}(x_s\, P_{sa} + (N_s - N_c)x_t\, P_{ta} + N_c M_s P_m^1 + (N_s - N_c)(M_s - M_c)\, P_m^2) \quad (41)$$

The relation between the probability of error for subcarrier index detection, P_e^{sd}, and the bit error rate probability of the subcarrier index bits, P_{sa}, may be defined as

$$P_{sa} = \frac{2^{(x_s-1)}}{2^{x_s}-1}\ P_e^{sd}, \quad (42)$$

and the bit error rate probability of the time slot index bits, P_{ta}, may be expressed as

$$P_{ta} = \frac{2^{(x_t-1)}}{2^{x_t}-1} P_T, \quad (43)$$

where P_T is connected to P_e^{sd} (the error probability of subcarrier index detection), and P_e^{td} (the error probability of the time slot index detection). The impact is evident, particularly when the detection of the subcarrier index is accurate; then $P_T = P_e^{td}$. While the average BER for index detection of time slot is analysed in the context of subcarrier index errors when subcarrier index detection is inaccurate. As a result, P_T is expressed as

$$P_T = \left(1 - P_e^{sd}\right)P_e^{td} + P_e^{sd}\left(\frac{\sum_{i=1}^{N_c}\binom{N_c}{i}(\,\bar{v}\, i + (N_s - N_c - i)P_e^{td})}{\sum_{i=1}^{N_c}\binom{N_c}{i}(N_s - N_c)}\right), \quad (44)$$

where $\bar{v} = \frac{2^{x_t-1}}{2^{x_t}}$ refers to the probability of error tied to the index detection of time slot inside of the subcarrier that has been erroneously detected. The bit error rate of the modulated information bits transmitted by active subcarriers P_m^1 can be calculated by P_e^{sd} and P_e^{md} as follows:

$$P_m^1 = \left(1 - P_e^{sd}\right)P_e^{md} + 0.5\, P_e^{sd} \quad (45)$$

Additionally, the bit error rate of the modulated information bits which are transmitted by unselected time slots of inactive subcarriers linked to P_e^{sd}, P_e^{td} and P_e^{md} can be described as:

$$P_m^2 = \left(1 - P_e^{sd}\right)\left[\left(1 - P_e^{td}\right)P_e^{md} + \frac{P_e^{td}}{2}\right] + P_e^{sd}\left[\frac{\sum_{i=1}^{N_c}\binom{N_c}{i}\left[\frac{i}{2} + (N_s - N_c - i)\left(\left(1 - P_e^{td}\right)P_e^{md} + \frac{P_e^{td}}{2}\right)\right]}{\sum_{i=1}^{N_c}\binom{N_c}{i}(N_s - N_c)}\right] \quad (46)$$

Under multipath Rayleigh fading channel condition, the final result of the average BER formula of the GJSTIM-DCSK may be defined as:

$$\overline{BER}_{\substack{GJSTIM \\ -DCSK}} = \int_0^\infty BER_{GJSTIM-DCSK} \cdot f(\gamma_b)\, d\gamma_b, \quad (47)$$

where $f(\gamma_b)$ is the probability density function of γ_b and which is expressed as:

$$f(\gamma_b) = \frac{{\gamma_b}^{L-1}}{(L-1)!\overline{\gamma_e}^L} exp\left(-\frac{\gamma_b}{\overline{\gamma_e}}\right), \quad (48)$$

where $\overline{\gamma_e} = \frac{E_b}{N_0}E({\alpha_l}^2)$ with $\sum_{l=1}^{L} E({\alpha_l}^2)$=1.

5. Simulation results

To validate the proposed system, we conducted several Monte Carlo simulations in this section. Simulations conducted under both Rayleigh fading channels and AWGN demonstrated a strong concordance between analytical and simulated results. Initially, we assessed the impact of varying system factors on the GJSTIM-DCSK'BER. Subsequently, we highlighted the advantages of our scheme by comparing its BER performance with that of other dual index modulation systems aided DCSK modulation. The multipath Rayleigh fading channel is uniformly represented in all figures as a three-channel with equal gains, where $E({\alpha_l}^2) = 1/3$ for $l = 1, 2, 3$, and path delays are $\tau_1 = 0, \tau_2 = 1$, and$\tau_3 = 2$. Significantly, the channel simplifies to an AWGN channel when $L = 1$, $\alpha_1 = 1$, and $\tau_1 = 0$.

5.1. BER performance evaluation

The GJSTIM-DCSK's BER performance with varying θ is clarified in Fig. 8. It is obvious that the GJSTIM-DCSK's BER increases as θ increases from 64 to 256. The system undergoes a gradual decline. For instance, where the BER is equal to 10^{-3}, the suggested system with θ=64 can achieve a gain in performance of approximately 1.25 dB and 1.75 dB in comparison to that of θ=256 over AWGN and Rayleigh fading channels, respectively. This effect may be associated to the increased noise-to-noise correlation caused by higher values of θ, resulting in an impoverished BER performance. Also the time-delay effects of the multipath Rayleigh channel mostly causes a somewhat poor alignment between the theoretical and simulated curves for smaller values of θ. The two curves can only completely match when θ is sufficiently large, because the GA approach cannot take time delay into account while calculating the system's BER and the distribution of decision variable doesn't strictly Conform to a Gaussian distribution when θ is small. The impact of time delay on the multipath Rayleigh fading channel reduces to a certain degree as θ rises.

The GJSTIM-DCSK' BER performance with varying M_s is illustrated in Fig. 9. The performance of the recommended method consistently enhances as M_s increases from 2 to 8, with other variables held constant. For example, the proposed GJSTIM-DCSK scheme with M_s=8 yields roughly 1 dB and 1.75 dB performance enhancements over AWGN and Rayleigh fading channels, respectively, at a BER is equal to 10^{-3}.

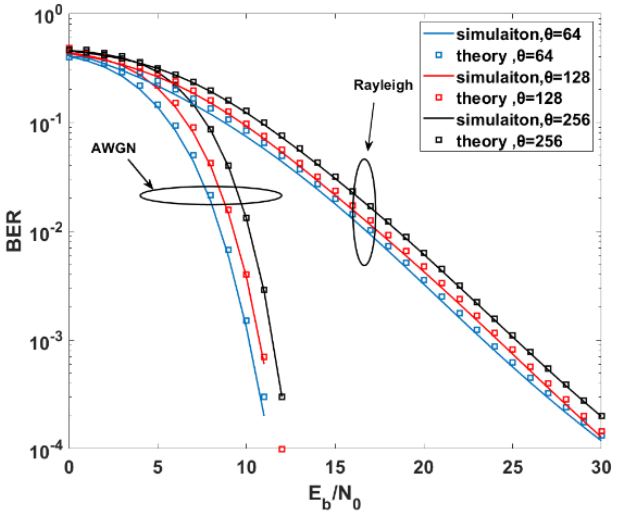

Figure. 8 GJSTIM-DCSK's BER Performance versus E_b/N_0 over AWGN and multipath Rayleigh fading channels with θ=64, 128, 256, G=4, $N_s = 8$, $N_c = 4$, $M_s = 8$, and $M_c = 4$

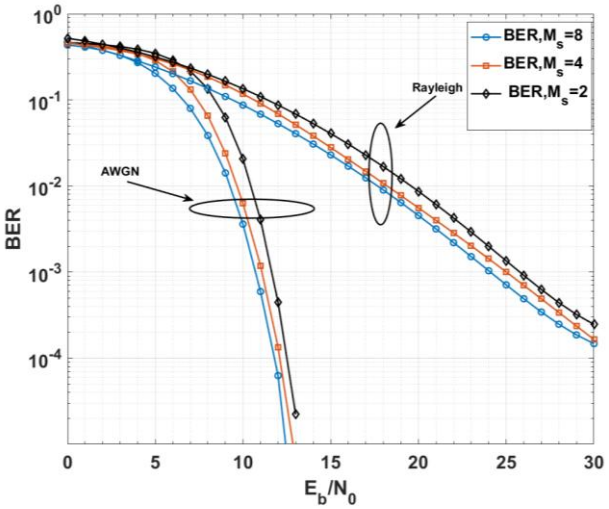

Figure. 9 GJSTIM-DCSK's BER Performance versus E_b/N_0 over AWGN and multipath Rayleigh fading channels with$M_s = 2, 4, 8$, $M_c = M_s/2$, G=4, $N_s = 8$, $N_c = 4$, and $\theta = 128$

This enhancement results from an increasing in transmitted bits, thereby enhancing the bit rate and bandwidth efficiency of the suggested scheme, which subsequently enhances the BER performance.

5.2. BER performance comparison

Fig. 10 shows the GJSTIM-DCSK'BER performance in comparison to the CTIM- DCSK, GFTIM-DCSK-II, and GSPIM-DCSK-II scheme at approximately a comparable data rate and the same β. The variables of the GJSTIM-DCSK scheme are set up as: $N_s = 4$, $N_c = 2$,$M_s = 8$, $M_c = 4$, G=4; for the CTIM-DCSK system: $N_s = 16$, $M_s = 8$,for the GFTIM-DCSK-II system: $N_s = 4$, $M_s = 8$, G=4, for the GSPIM-DCSK-II system: $N_s = 2$, $N_p = 8$ and G=4. The relevant data rates are $152/\beta T_c$, $112/\beta T_c$, $144/\beta T_c$ and $160/\beta T_c$ under the previously indicated parameter combinations. The figure's observations reveal that the GJSTIM-DCSK scheme shows inferior performance relative to the CTIM DCSK scheme over Rayleigh fading channel and AWGN circumstances. Nonetheless, in comparison to the GFTIM-DCSK-II and GSPIM-DCSK-II schemes, the GJSTIM-DCSK system still has distinct advantages, where the performance of GJSTIM-DCSK is roughly 1.5 dB and 0.5 dB superior to GFTIM-DCSK-II and GSPIM-DCSK-II under AWGN, and 3.5 dB and 3 dB under Rayleigh fading channels, respectively, at BER of 10^{-3}.

Subsequently, we performed a contrast of the GJSTIM-DCSK's BER performance with two other structurally similar systems that employ dual index

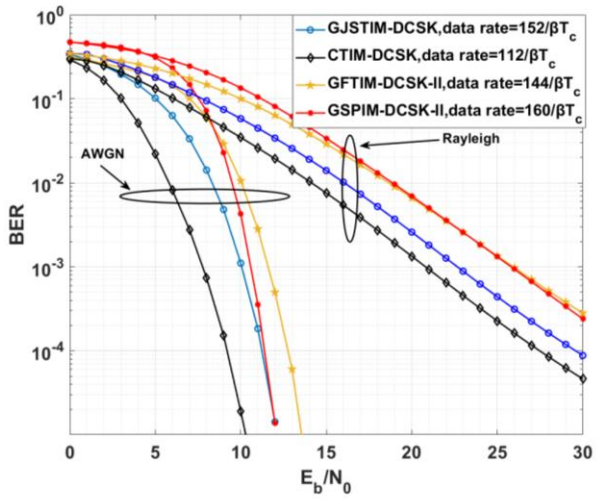

Figure. 10 the GJSTIM-DCSK' BER performance and other Schemes with approximately a comparable data rate over AWGN and multipath Rayleigh fading channels and β=256

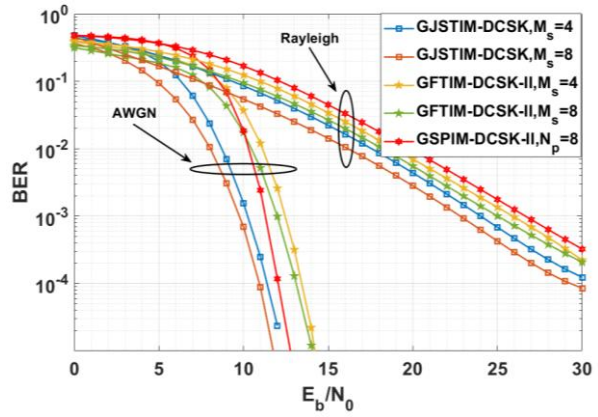

Figure. 11 BER Performance comparison between GJSTIM-DCSK and Other DCSK modulation Scheme with Different M_s

modulation as illustrate in Fig. 11. These comparisons were performed under identical conditions, including carriers and time slots. In particular, we compared between our system and GFTIM-DCSK-II and GSPIM-DCSK-II for varying time slots, while maintaining the same other parameters for all systems. The primary simulation parameters for all systems are as follows: $N_s = 8$, $N_c = 4$, $M_c = M_s/2$, $N_p = 8$, G=4, and $\beta = 256$.

Fig. 11 illustrates that the GJSTIM-DCSK's BER performance surpasses that of the other schemes over multipath Rayleigh fading channels and AWGN as the time slots number (M_s) increases. For instance, at M_s =4 and BER=10^{-3} under both Rayleigh fading channels and AWGN, the GJSTIM-DCSK scheme exhibits an estimated 2dB gain over the GFTIM-DCSK-II, while showing gains of 1dB and 2.5dB over the GSPIM-DCSK-II under AWGN and Rayleigh fading channels, respectively. As MS rises from 4 to 8, the GJSTIM-DCSK system exhibits a performance enhancement of roughly 2.25 dB and 2 dB contrast to GFTIM-DCSK-II over AWGN and Rayleigh fading channels, respectively, and outperforms GSPIM-DCSK-II by 1.5 dB in AWGN and 3.5 dB in Rayleigh fading channels.

6. Complexity analysis

The complexity of the system can be categorized into two components: complexity of multiplication and complexity of search. Complexity of multiplication denotes the quantity of multiplications necessary for the modulation and demodulation of information bits. In contrast, search complexity relates to the number of contrast processes needed to identify the activation sequence of transmission resources, such time slots as and carriers [56, 62] .

To modulate the signals, the proposed GJSTIM-DCSK system transmitter requires $N_c M_s \theta + (M_s\_M_c)(N_s - N_c)\theta$ multiplications. According to the demodulation procedure at the receiver, the number of multiplication operations is $N_s M_s \theta + (N_s - N_c) M_s \theta$, while search complexity is $\binom{N_s}{N_c} + (N_s - N_c)\binom{M_s}{M_s - M_c}$. A description of each system's complexity is given in Table 4, where $O_{GJSTIM} = N_C M_S \theta + (M_S - M_C)(N_S - N_C)\theta + N_S M_S \theta + (N_S - N_C) M_S \theta + \binom{N_s}{N_c} + (N_S - N_C)\binom{M_s}{M_s - M_c}$ represents the complexity of proposed system, and the remaining systems' complexities are discovered by the previously specified complexity calculation approach. For varying values of θ, Fig. 12 shows the complexity per transmitted bit of the suggested scheme and other scheme. Every scheme has the same parameters: $M_s = 4$, $M_c = 2$, $N_s = 4$,$N_c = 2$, $N_p = 8$, and G=8. Consequently, the bits number sent regarding the listed system is 144, 152, 40, 112, 13, 5, 4, and 1, respectively. It is clearly that the complexity of the suggested scheme higher than that of the GFTIM-DCSK-II, GSIM-DCSK-II and GSPIM-DCSK-II schemes, but it's less than that of the other schemes. Through employing the Hilbert transform in both the transmitter and receiver of the GJSTIM-DCSK scheme, we can mitigate interference noise and improve system performance.

Additionally, using of k-combinatorial mapping to select N_c subcarriers out of N_s total subcarrier and to select M_c time slots out of M_s , helps to accomplish the high bit rate and bandwidth efficiency

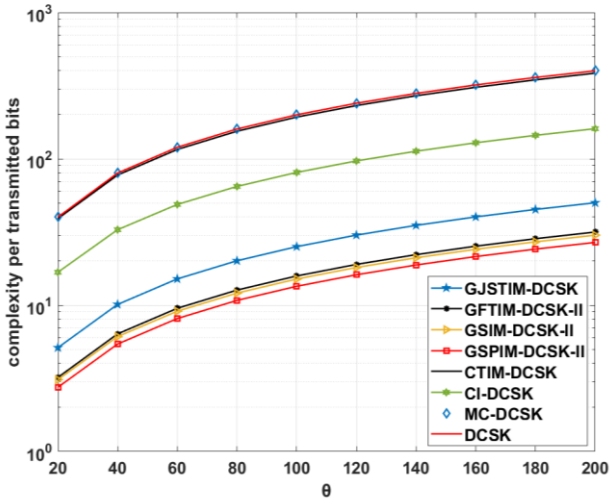

Figure. 12 The complexity per transmitted bit comparisons with different θ

Table 4. the GJSTIM-DCSK's complexity in comparison with other modulations

System	Complexity
GJSTIM_DCSK	O_{GJSTIM}
GFTIM_DCSK_II [58]	$2(N_S-1)M_S\theta+\binom{N_s}{1}+\binom{M_s}{1}$
GSIM_DCSK_II [52]	$2(N_S-1)\theta+\binom{N_s}{1}$
GSPIM_DCSK_II [59]	$(N_S-1)\theta+(N_S-1)N_p\theta+\binom{N_s}{1}+\binom{N_p}{1}$
CTIM_DCSK [56]	$[(N_S-1)(M_S-1)+N_SM_S]\theta+\binom{N_s}{1}+\binom{M_s}{1}$
CI_DCSK [44]	$N_S\theta+\binom{N_s}{1}$
MC_DCSK [30]	$2N_S\theta$
DCSK [7]	2θ

Table 5. Comparison of the hardware complexity for several DCSK modulations at transmitter and receiver

Hardware component	Proposed system GJFTIM-DCSK	GFTIM-DCSK-II [58]	GSIM-DCSK-II [52]	GSPIM-DCSK-II [59]	CTIM-DCSK [56]
Adder	1	1	1	1	N_s+1
Multipliers	$3GN_s+2$	$3GN_s+2$	$3GN_s+2$	$G(N_s+N_pN_s)+2GN_S+2$	N_s
Index mapper /selector	2G	2G	G	2G	2
Pulse Shaping Filter	GN_s+1	GN_s+1	GN_s+1	GN_s+1	N_s+1
Hilbert Filter	1	0	0	0	0
Matched Filter	GN_s+1	GN_s+1	GN_s+1	GN_s+1	N_s
Energy Detector	GN_sM_s	GN_sM_s	GN_s	GN_s	N_sM_s
Permutation Block	0	0	0	2	0

as demonstrated in Figs 4, to 7. However, this is also producing an increase in system complexity. Thus, this increased complexity is a trade-off for higher performance, transmission bits rate, and bandwidth efficiency. While suggested GJSTIM-DCSK scheme exhibits greater hardware complexity, it offers improved bits rate and bandwidth efficiency over other comparable systems. Tables 5 provide a breakdown of the components used to evaluate the transmitter and receiver complexity for GJSTIM-DCSK, GFTIM-DCSK-II, GSIM-DCSK-II, GSPIM-DCSK-II, and CTIM-DCSK.

7. Conclusion

This system is the first DCSK implementation that integrates a grouping technique with integer K-mapping to increase the index and modulated bits. These approaches facilitate enhanced bits rates and bandwidth efficiency. The GJSTIM-DCSK system adds a receiver noise reduction mechanism and Hilbert transform in order to enhance BER performance. The derived BER formula for AWGN and multipath Rayleigh fading channels demonstrates a robust correlation with simulation results, validating the exactness of this formula. In addition, the GJSTIM-DCSK scheme is proven to be superior to conventional DCSK systems through an evaluation of data rates and spectrum efficiency. Compared to similar systems, our proposed system works better as the sub-blocks and time slots number goes up in terms of bits rates and bandwidth efficiency, where bandwidth efficiency improved by roughly 1.33 , 1.45 and 5.5 times than that of GFTIM-DCSK-II , CTIM-DCSK and GSPIM-DCSK-II, respectively with N_s =16, N_c =1, $M_s=16$, $M_c=4$, G=2

Furthermore, a comparison with similar structural systems such as GFTIM-DCSK-II and GSPIM-DCSK-II, operating at the same bits rate and under varying time slot conditions, demonstrates the superior error performance of the GJSTIM-DCSK scheme. the GJSTIM-DCSK scheme exhibits an estimated 2dB gain over the GFTIM-DCSK-II over both Rayleigh fading and AWGN channels, at M_s =4 and BER=10^{-3}, while showing gains of 1dB and 2.5dB over the GSPIM-DCSK-II in AWGN and Rayleigh fading channels, respectively. However, our suggested system lags behind CTIM-DCSK in terms of BER. but the GJSTIM-DCSK scheme is superior in terms of other evaluated factors. With all of these features, the suggested GJSTIM-DCSK scheme can function as an effective communication system for high bits rate transmission situations. In future work, to enhance the BER, LDPC or polar codes will be combined. Additionally, to improve the data rate, new dimensions may be added, such as using the permutation index of chaotic signals for index modulation.

Notation list

Symbol	Definition
C_x	Reference-chaotic signal
θ	Length of the reference-chaotic signal
C_y	Orthogonal chaotic signal
G	Number of sub-blocks in the system
M_s	Number of time slots in each sub-block
N_s	Number of subcarriers in each sub-block
M_c	Number of selected time slots in each sub-block
N_c	Number of active subcarriers in each sub_block
x_s	Subcarrier index bits
x_t	Time slot index bits
F_c^{g}	active subcarriers indices in g^{th}
F_t^{g}	Selected time slots indices
$\widetilde{F_t^{\mathrm{g}}}$	complement of F_t^{g}
C_x^r	Repeated reference-chaotic signal
AWGN	Additive White Gaussian Noise
$s(t)$	Transmitted signal
$r(t)$	Received signal
R_x	averaged received chaos reference
$\widetilde{n_R}$	AWGN corresponding to R_x
R_y	orthogonal vector of R_x
ζ_c^{g}	Detected index of active subcarriers in g^{th} sub_block
T_s	k-combinatorial mapping of the subcarriers
T_t	k-combinatorial mapping of the time slots
$\widetilde{\zeta_c^{\mathrm{g}}}$,	complement of ζ_c^{g}
$\widetilde{\zeta_{tt}^{\mathrm{g}}}$	Matrix of detected unselected time slots at receiver
ζ_{tt}^{g}	Matrix of detected selected time slots at receiver
α_l	channel coefficient of l^{th}path in multipath Rayleigh fading channel
τ_l	path delay of the l^{th}path in multipath Rayleigh fading channel
$n_l^{i,j}$	AWGN added to information signal in i subcarrier and j time slot
μ	Mean value
σ	Variance
P_e^{sd}	Error Rate Probability of Subcarrier Index Detection
P_e^{td}	Error Rate Probability of Time-Slot Index Detection
P_e^{md}	Error Rate Probability of Modulated Bits
P_{sa}	bit error rate probability of the subcarrier index bits
P_{ta}	bit error rate probability of the time slot index bits
P_m^1	bit error rate probability of the modulated bits transmitted by all time slots of active subcarriers
P_m^2	bit error rate probability of the modulated bits transmitted by unselected time slots of inactive subcarriers
BER	Bit error rate of the system

Conflicts of Interests

The authors declare no conflict of interest.

Author Contribution

The first author performed conceptualization, methodology, software, formal analysis, resources, data curation, and writing—original draft preparation. The second author assumed the role of supervision, performed a comprehensive work review, and conducted the process of validation.

Acknowledgments

This work was supported by the Mustansiriyah University, College of Engineering.

References

[1] M. Sushchik, L. S. Tsimring, and A. R. Volkovskii, "Performance analysis of correlation-based communication schemes utilizing chaos", *IEEE Transactions on Circuits and Systems I Fundamental Theory and Applications*, Vol. 47, No. 12, pp. 1684–1691, 2000.

[2] A. P. Kurian, S. Puthusserypady, and N. S. M. Htut, "Performance enhancement of DS/CDMA system using chaotic complex spreading sequence", *IEEE Transactions on Wireless Communications*, Vol. 4, No. 3, pp. 984–989, 2005.

[3] A. Abel and W. Schwarz, "Chaos communications-principles, schemes, and system analysis", *Proceedings of the IEEE*, Vol. 90, No. 5, pp. 691–710, 2002.

[4] G. Kaddoum and N. Tadayon, "Differential Chaos Shift Keying: A Robust Modulation Scheme for Power-Line Communications", *IEEE Transactions on Circuits & Systems II Express Briefs*, Vol. 64, No. 1, pp. 31–35, 2016.

[5] G. Kaddoum, H.-V. Tran, L. Kong, and M. Atallah, "Design of Simultaneous Wireless Information and Power Transfer Scheme for Short Reference DCSK Communication Systems", *IEEE Transactions on Communications*, p. 1, 2016.

[6] G. Kaddoum, "Wireless Chaos-Based Communication Systems: A Comprehensive Survey", *IEEE Access*, Vol. 4, pp. 2621–2648, 2016.

[7] G. Kolumb´an, B. Vizv´ari, W. Schwarz, and A. Abel, "Differential chaos shift keying: A robust coding for chaos communication", In: *Proc. of NDES*, Vol. 96, pp. 87–92, 1996.

[8] Y. Xia, C. K. Tse, and F. C. M. Lau, "Performance of Differential Chaos-Shift-Keying Digital Communication Systems Over a Multipath Fading Channel With Delay Spread*", IEEE Transactions on Circuits and Systems II Analog and Digital Signal Processing*, Vol. 51, No. 12, pp. 680–684, 2004.

[9] S. Wang, S. Lu, and E. Zhang, "MIMO-DCSK communication scheme and its performance analysis over multipath fading channels", *Journal of Systems Engineering and Electronics*, Vol. 24, No. 5, pp. 729–733, 2013.

[10] H. Li and N. S. F. Feng, "UWB DCSK system design and simulation", In: *Proc. of International Conference on Test and Measurement*, Vol. 32, pp. 311–314, 2009.

[11] Y. Yu-Wang, "FM-DCSK UWB System Design and Its Performance Analysis in Multipath Channel", *Journal of Nanjing University of Science and Technology*, 2008.

[12] G. Kaddoum and M. El-Hajjar, "Analysis of Network Coding Schemes for Differential Chaos Shift Keying Communication System", *arXiv (Cornell University)*, 2015.

[13] Y. Fang, W. Chen, P. Chen, Y. Tao, and M. Guizani, "SR-DCSK cooperative communication system with code index modulation: A new design for 6G new radios", *China Communications*, Vol. 20, No. 10, pp. 1–16, 2023.

[14] W. Xu, L. Wang, and G. Chen, "Performance of DCSK Cooperative Communication Systems Over Multipath Fading Channels", *IEEE Transactions on Circuits and Systems I Regular Papers*, Vol. 58, No. 1, pp. 196–204, 2010.

[15] B. Nazar and F. S. Hasan, "Performance analysis of two-way multi-users cooperative communication system based on GSPIM-DCSK scheme", *AEU - International Journal of Electronics and Communications*, Vol. 178, p. 155303, 2024.

[16] S. J. Sarkar and P. K. Kundu, "A novel DCSK communication scheme for PLCC based DAS", In: *Proc. of 8th International Conference on Electrical and Computer Engineering*, 2014.

[17] V. Mohan, A. Mathur, and G. Kaddoum, "Analyzing Physical-Layer Security of PLC Systems Using DCSK: A Copula-Based Approach", *IEEE Open Journal of the Communications Society*, Vol. 4, pp. 104–117, 2022.

[18] L. Lazović, A. Jovanović and V. Rubežić, "Performance Analysis of an Underwater Acoustic Communication System Based on DCSK Modulation", In: *Proc. of 27th International Conference on Information Technology (IT)*, Zabljak, Montenegro, pp. 1-4, 2023.

[19] H. Dedieu, M. P. Kennedy, and M. Hasler, "Chaos shift keying: modulation and demodulation of a chaotic carrier using self-synchronizing Chua's circuits", *IEEE Transactions on Circuits and Systems II Analog and Digital Signal Processing*, Vol. 40, No. 10, pp. 634–642, 1993.

[20] H. Yang and G.-P. Jiang, "High-Efficiency Differential-Chaos-Shift-Keying Scheme for Chaos-Based Noncoherent Communication", *IEEE Transactions on Circuits & Systems II Express Briefs*, Vol. 59, No. 5, pp. 312–316, 2012.

[21] W. K. Xu, L. Wang, and G. Kolumbán, "A novel differential chaos shift keying modulation scheme", *International Journal of Bifurcation and Chaos*, Vol. 21, No. 03, pp. 799–814, 2011.

[22] G. Kaddoum and F. Gagnon, "Design of a High-Data-Rate Differential Chaos-Shift Keying System", *IEEE Transactions on Circuits & Systems II Express Briefs*, Vol. 59, No. 7, pp. 448–452, 2012.

[23] W. Xu, L. Wang, and C.-Y. Chi, "A Simplified GCS-DCSK Modulation and Its Performance Optimization", *International Journal of Bifurcation and Chaos*, Vol. 26, No. 13, p. 1650213, 2016.

[24] Y. Lu, M. Miao, L. Wang, and W. Xu, "A Multilevel Code-Shifted Differential Chaos Shift Keying System With Reference Diversity", *IEEE Transactions on Circuits & Systems II Express Briefs*, Vol. 67, No. 11, pp. 2462–2466, 2020.

[25] G. Kaddoum, E. Soujeri, C. Arcila, and K. Eshteiwi, "I-DCSK: An Improved Noncoherent Communication System Architecture", *IEEE Transactions on Circuits & Systems II Express Briefs*, Vol. 62, No. 9, pp. 901–905, 2015.

[26] L. Wang, G. Cai, and G. R. Chen, "Design and performance analysis of a new multiresolution M-ary differential chaos shift keying communication system", *IEEE Transactions on Wireless Communications*, Vol. 14, No. 9, pp. 5197–5208, 2015.

[27] G. Cai, Y. Fang, G. Han, F. C. M. Lau, and L. Wang, "A Square-Constellation-Based M-ary DCSK Communication System", *IEEE Access*, Vol. 4, pp. 6295–6303, 2016.

[28] G. Cai, Y. Fang, and G. Han, "Design of an Adaptive Multiresolution M-ary DCSK System", *IEEE Communications Letters*, Vol. 21, No. 1, pp. 60–63, 2016.

[29] Y. Tan, W. Xu and S. Hong, "An M-ary code shifted differential chaos shift keying scheme", In: *Proc. of 23rd Asia-Pacific Conference on Communications (APCC)*, Perth, WA, Australia, pp. 1-6, 2017.

[30] G. Kaddoum, F.-D. Richardson, and F. Gagnon, "Design and Analysis of a Multi-Carrier Differential Chaos Shift Keying Communication System", *IEEE Transactions on Communications*, Vol. 61, No. 8, pp. 3281–3291, 2013.

[31] H. Yang and G.-P. Jiang, "Reference-Modulated DCSK: A Novel Chaotic Communication Scheme", *IEEE Transactions on Circuits & Systems II Express Briefs*, Vol. 60, No. 4, pp. 232–236, 2013.

[32] G. Kaddoum, E. Soujeri, and Y. Nijsure, "Design of a Short Reference Noncoherent Chaos-Based Communication Systems", *IEEE Transactions on Communications*, Vol. 64, No. 2, pp. 680–689, 2016.

[33] T. J. Wren and T. C. Yang, "Orthogonal chaotic vector shift keying in digital communications", *IET Communications*, Vol. 4, No. 6, p. 739-753, 2010.

[34] F. S. Hasan, "Design and Analysis of an Orthogonal Chaotic Vectors based Differential Chaos Shift Keying Communication System", *Al-Nahrain Journal for Engineering Sciences*, Vol. 20, No. 4, p. 952-958, 2017.

[35] G. Kaddoum and E. Soujeri, "NR-DCSK: A Noise Reduction Differential Chaos Shift Keying System", *IEEE Transactions on Circuits & Systems II Express Briefs*, Vol. 63, No. 7, pp. 648–652, 2016.

[36] F. S. Hasan, "Design and Analysis of an OFDM-Based Short Reference Quadrature Chaos Shift Keying Communication System", *Wireless Personal Communications*, Vol. 96, No. 2, pp. 2205–2222, 2017.

[37] Z. Liu, L. Zhang, Z. Wu, and J. Bian, "A Secure and Robust Frequency and Time Diversity Aided OFDM–DCSK Modulation System Not Requiring Channel State Information", *IEEE Transactions on Communications*, Vol. 68, No. 3, pp. 1684–1697, 2019.

[38] F. S. Hasan and A. A. Valenzuela, "Design and Analysis of an OFDM-Based Orthogonal Chaotic Vector Shift Keying Communication System", *IEEE Access*, Vol. 6, pp. 46322–46333, 2018

[39] F. S. Hasan, M. J. Zaiter, and R. A. Mohammed, "Design and Analysis of a Wavelet Packet Modulation Based Differential Chaos Shift Keying Communication System", *Wireless Personal Communications*, Vol. 109, No. 4, pp. 2439–2450, 2019.

[40] Z. Chen, L. Zhang, W. Wang, and Z. Wu, "A Pre-Coded Multi-Carrier M-Ary Chaotic Vector Cyclic Shift Keying Transceiver for Reliable Communications", *IEEE Transactions on Wireless Communications*, Vol. 21, No. 2, pp. 1007–1021, 2021.

[41] E. Basar, "Index modulation techniques for 5G wireless networks", *IEEE Communications Magazine*, Vol. 54, No. 7, pp. 168–175, 2016.

[42] W. Xu and L. Wang, "CIM-DCSK: A differential chaos shift keying scheme with code-index modulation", In: *Proc. Of 16th International Symposium on Communications*

and Information Technologies (ISCIT), Qingdao, China, pp. 100-104, 2016.

[43] W. Xu, Y. Tan, F. C. M. Lau, and G. Kolumban, "Design and Optimization of Differential Chaos Shift Keying Scheme With Code Index Modulation", *IEEE Transactions on Communications*, Vol. 66, No. 5, pp. 1970–1980, 2018.

[44] G. Cheng, L. Wang, W. Xu, and G. Chen, "Carrier Index Differential Chaos Shift Keying Modulation", *IEEE Transactions on Circuits & Systems II Express Briefs*, Vol. 64, No. 8, pp. 907–911, 2016.

[45] W. Dai, H. Yang, Y. Song, and G. Jiang, "Two-Layer Carrier Index Modulation Scheme Based on Differential Chaos Shift Keying", *IEEE Access*, Vol. 6, pp. 56433–56444, 2018.

[46] M. Herceg, G. Kaddoum, D. Vranjes, and E. Soujeri, "Permutation Index DCSK Modulation Technique for Secure Multiuser High-Data-Rate Communication Systems", *IEEE Transactions on Vehicular Technology*, Vol. 67, No. 4, pp. 2997–3011, 2017.

[47] W. Xu, T. Huang, and L. Wang, "Code-Shifted Differential Chaos Shift Keying with Code Index Modulation for High Data Rate Transmission", *IEEE Transactions on Communications*, Vol. 65, No. 10, p. 4285-4294, 2017.

[48] Y. Tan, W. Xu, T. Huang, and L. Wang, "A Multilevel Code Shifted Differential Chaos Shift Keying Scheme With Code Index Modulation", *IEEE Transactions on Circuits & Systems II Express Briefs*, Vol. 65, No. 11, pp. 1743–1747, 2017.

[49] X. Cai, W. Xu, L. Wang, and F. Xu, "Design and Performance Analysis of Differential Chaos Shift Keying System With Dual-Index Modulation", *IEEE Access*, Vol. 7, pp. 26867–26880, 2019.

[50] X. Cai, W. Xu, F. C. M. Lau, and L. Wang, "Joint Carrier-Code Index Modulation Aided M-ary Differential Chaos Shift Keying System", *IEEE Transactions on Vehicular Technology*, Vol. 69, No. 12, pp. 15486–15499, 2020.

[51] H. Yang, S.-Y. Xu, and G.-P. Jiang, "A High Data Rate Solution for Differential Chaos Shift Keying Based on Carrier Index Modulation", *IEEE Transactions on Circuits & Systems II Express Briefs*, Vol. 68, No. 4, pp. 1487–1491, 2020.

[52] F. S. Hasan, "Design and analysis of grouping subcarrier index modulation for differential chaos shift keying communication system", *Physical Communication*, Vol. 47, p. 101325, 2021.

[53] X. Cai, W. Xu, S. Hong, L. Wang, and L. Zhang, "General Carrier Index Aided Dual-Mode Differential Chaos Shift Keying With Full Mapping: Design and Optimization", *IEEE Transactions on Vehicular Technology*, Vol. 70, No. 11, pp. 11665–11677, 2021.

[54] X. Cai, W. Xu, L. Wang, and G. Chen, "Towards High-Data-Rate Noncoherent Chaotic Communication: A Multiple-Mode Differential Chaos Shift Keying System", *IEEE Transactions on Wireless Communications*, Vol. 20, No. 8, pp. 4888–4901, 2021.

[55] G. Zhang, X. Chen, and R. Lai, "Joint Time-Slot Configuration and Discrete W Transform for Dual-Mode Index Modulation DCSK System with Noise Reduction", *IEEE Transactions on Communications*, p. 1, 2024.

[56] Y. Fang, J. Zhuo, H. Ma, S. Mumtaz, and Y. Li, "Design and Analysis of a New Index-Modulation-Aided DCSK System With Frequency-and-Time Resources", *IEEE Transactions on Vehicular Technology*, Vol. 72, No. 6, pp. 7411–7425, 2023.

[57] R. A. Yaseen and F. S. Hasan, "Design and Analysis of Grouping Active Subcarrier Frequency-Time Index Modulation for Differential Chaos Shift Keying Communication System", *Journal of Communications Software and Systems*, Vol. 20, No. 2, pp. 173–185, 2024.

[58] R. Abdulkareem and F. Hasan, "Design and Analysis of Grouping Non-Active Frequency - Time Index Modulation for Differential Chaos Shift Keying Communication System", *International Journal of Intelligent Engineering and Systems*, Vol. 17, No. 3, pp. 744–757, 2024.

[59] B. Nazar and F. S. Hasan, "Joint Grouping Subcarrier and Permutation Index Modulations Based Differential Chaos Shift Keying System", *Physical Communication*, Vol. 61, p. 102213, 2023.

[60] E. Basar, U. Aygolu, E. Panayirci, and H. V. Poor, "Orthogonal Frequency Division Multiplexing With Index Modulation", *IEEE Transactions on Signal Processing*, Vol. 61, No. 22, pp. 5536–5549, 2013.

[61] H. Ma, Y. Fang, P. Chen, S. Mumtaz, and Y. Li, "A Novel Differential Chaos Shift Keying Scheme With Multidimensional Index Modulation", *IEEE Transactions on Wireless Communications*, Vol. 22, No. 1, pp. 237–256, 2022.

[62] G. Zhang, X. Wu, Y. Yang, and S. Shao, "Design and Analysis of High Data Rate Four-Dimensional Index Modulation for Differential Chaos Shift Keying System", *IEEE Transactions on Wireless Communications*, Vol. 23, No. 9, pp. 12455–12468, 2024.

[63] F. S. Hasan and A. A. Valenzuela, "Joint Subcarrier Time Reference Index Modulation aided Differential Chaos Shift Keying Communication System", *IEEE Access*, Vol. 12, p. 159935-159951, 2024.